applied sciences

MDPI

Article

Exergoeconomic Analysis of a Gas Turbine Integrated with Supercritical CO_2 Energy Storage and Cascade Heat Utilization Considering Different Operating Periods

Luyi Tan [1], Xikai Liu [2], Ding Wang [2], Yonghui Xie [2,*] and Di Zhang [2]

[1] Shanghai XuanYuan Power Technology Co., Ltd., Shanghai 200240, China; tly84930@163.com
[2] School of Energy and Power Engineering, Xi'an Jiaotong University, Xi'an 710049, China
* Correspondence: yhxie@mail.xjtu.edu.cn; Tel.: +86-029-82664443

Abstract

With the increasing integration of renewable energy, large-scale energy storage systems are required to improve the flexibility of energy supply and alleviate the mismatch between power generation and demand. However, the performance evaluation of integrated energy systems combining continuous power generation and periodically operated energy storage remains challenging due to the different operating time scales of individual subsystems. In this study, a gas turbine integrated molten salt thermal energy storage and supercritical CO_2 energy storage (GT-TES-CCES) system with cascade heat utilization is proposed. The proposed system recovers high-temperature exhaust heat from the gas turbine through molten salt storage, provides thermal input for CO_2 expansion during discharge, and further utilizes residual heat for hot water production. A comprehensive thermodynamic and exergoeconomic model is developed, and a unified 24 h evaluation framework is introduced to consistently evaluate the continuously operated gas turbine subsystem and periodically operated charging/discharging processes. The SPECO method is employed to investigate the exergy cost formation and transfer characteristics, and multi-objective optimization is performed to identify the trade-off between exergy efficiency and product cost. At the nominal operating point, the proposed system achieves an electrical efficiency of 48.71%, an overall energy efficiency of 75.97%, and an exergy efficiency of 50.29%, with an instantaneous net power output of 40.26 MW during the discharge period and useful hot water production of 14.13 MW. After multi-objective optimization, the electrical efficiency and exergy efficiency increase to 53.99% and 54.82%, corresponding to improvements of 10.84% and 9.01%. Meanwhile, the total unit product exergy cost decreases from 14.32 to 13.55 \$·GJ^{-1}, demonstrating the economic benefit of the optimized configuration. The results indicate that the proposed multi-period exergoeconomic framework provides an effective approach for evaluating and optimizing integrated energy systems involving continuous power generation and flexible energy storage.

Keywords: gas turbine; supercritical CO_2 energy storage; molten salt thermal energy storage; multi-objective optimization

Academic Editor: José A. Orosa García

Received: 5 October 2026
Revised: 23 October 2026
Accepted: 27 October 2026
Published: 2 November 2026

Copyright: © 2026 by the authors. Licensee MDPI, Basel, Switzerland. This article is an open access article distributed under the terms and conditions of the Creative Commons Attribution (CC BY) license.

1. Introduction

Growing deployment of renewable energy has exacerbated the discrepancy between variable electricity generation and demand. Large-scale energy storage is therefore playing an increasingly important role in improving power-system flexibility and renewable-energy utilization [1,2]. Among various energy storage technologies, CO_2-based energy storage systems are receiving increasing interest because of their favorable thermophysical properties, high energy storage density, and operational flexibility. Compared with conventional energy storage technologies, supercritical CO_2 exhibits favorable thermophysical properties and enables reversible compression and expansion processes, allowing effective decoupling between electricity consumption during charging and electricity production during discharge [1]. These characteristics make the system well suited to grid-scale energy storage with extended discharge durations. However, the performance of a standalone compressed CO_2 energy storage system (CCES) strongly depends on the management of compression heat and the heat required during the discharge process. Efficient integration with an appropriate thermal source is therefore important for improving both system performance and economic feasibility.

Gas turbine (GTs) provide a suitable energy source for integration with CCES systems because they can continuously supply electricity and high-temperature exhaust heat for hybrid energy storage applications [3–5]. The exhaust heat from GT can be recovered and stored using thermal energy storage (TES) systems. By coupling molten salt TES with CCES, the recovered exhaust heat can be stored during GT operation and subsequently released to provide the required thermal input for CO_2 expansion during electricity generation periods [6]. Several studies have investigated the integration of CCES with thermal storage technologies. Tang et al. [7] introduced high temperature TES into a CCES system and showed that thermal storage conditions strongly affect both thermodynamic and economic performance. Hao et al. [8] investigated a CCES system capable of simultaneously generating electricity and heat, demonstrating the potential of CO_2 storage systems for integrated energy supply. Studies on the integration of CO_2 cycles with conventional thermal power systems have also shown that effective matching between the exhaust heat source and the CO_2 cycle can significantly improve waste heat utilization [9]. In addition, recent studies have further combined Supercritical CO_2 (sCO_2) cycles with TES and waste heat recovery processes to improve system flexibility and thermal energy utilization [10]. However, most existing studies mainly focus on the thermodynamic improvement of individual CCES systems or the optimization of specific heat recovery processes. Limited attention has been paid to integrated systems involving multiple energy storage forms and different operating time scales. In practical applications, the GT subsystem may operate continuously to provide a stable energy source, whereas the CO_2 charging and discharging processes are usually determined by electricity demand characteristics and may only occur during specific periods. Meanwhile, the thermal energy recovered from GT exhaust and the compressed CO_2 stored during charging are transferred across different operating periods before being converted into electricity and useful heat. The interaction between continuous energy supply, intermittent energy storage, and flexible energy release introduces additional complexity to the system evaluation. Therefore, a comprehensive framework considering the multi-period characteristics of such integrated systems is required.

In addition to thermodynamic performance, the economic consequences of exergy destruction and equipment investment must also be considered for such highly integrated systems. Exergoeconomic analysis provides an effective way to connect these two aspects. Among the available methods, the Specific Exergy Costing (SPECO) approach provides a systematic framework for tracing cost formation and transfer among different components and energy streams. SPECO has already been applied to various power and

energy storage systems [11]. For example, recent research on adiabatic CAES used SPECO to quantify the influence of pressure ratio and system configuration on exergy-related costs [12]. Exergoeconomic analysis has also been applied to sCO_2 cycles and integrated thermal systems to identify components with high investment costs or high exergy-destruction costs [13]. Therefore, the main difficulty in applying SPECO to the present system is not the applicability of the method itself, but the treatment of different operating periods. In the GT-sCO_2 integrated system, the GT subsystem operates continuously, whereas the charging and discharging processes only occur during prescribed operating periods. Directly combining their exergy and cost rates without considering this difference may lead to an inconsistent system-level evaluation. Moreover, the thermal energy stored in molten salt and the compressed CO_2 stored during charging are transferred across different periods before being converted into electricity and useful heat. A consistent time basis and cost transfer relationship are therefore required to correctly describe the cost formation process of the entire system.

After establishing the thermodynamic and exergoeconomic models, determining an appropriate balance between system performance and economic cost is another important issue. Multi-objective optimization (MOO) has been widely used in advanced energy systems because improvements in thermodynamic performance are often accompanied by increased equipment investment and system cost. Tang et al. [7] performed thermo-economic MOO of a CCES system integrated with high-temperature TES. Other studies have applied MOO to CO_2 energy storage and sCO_2 power systems to identify the trade-off between efficiency and economic performance [14,15]. However, most optimization studies still evaluate charging and discharging processes under prescribed operating conditions and mainly focus on conventional thermodynamic variables such as pressure, temperature, and pressure ratio. For a GT-sCO_2 energy storage system, the situation is more complicated. Changes in the operating parameters not only affect the efficiency of the CO_2 cycle, but also change the amount of GT exhaust, the behavior of TES, the production of useful heat, and the cost distribution among different components. More importantly, the GT and energy-storage subsystems operate over different daily durations. The combined effects of these operating characteristics on the thermodynamic-economic Pareto frontier remain largely unexplored.

Motivated by the above research gaps, this paper proposes an integrated GT-TES-CCES system and cascade heat utilization, and conducts detailed thermodynamic, exergoeconomic and MOO analyses. The GT operates continuously, while the sCO_2 storage subsystem operates according to prescribed charging and discharging periods. Residual heat from the system is further recovered to produce useful hot water, allowing both electricity and heat to be regarded as final products. The key features of the present study are summarized as follows:

(1) An integrated GT-TES-CCES system with cascade thermal utilization is proposed. The GT exhaust heat is recovered and stored through molten salt TES, while supercritical CO_2 storage provides additional energy-shifting capability. In this way, electricity generation, energy storage, and heat supply are integrated within the same system.

(2) A multi-period SPECO-based exergoeconomic framework is established for an integrated energy-storage system with different operating durations. A unified 24 h evaluation basis is introduced to consistently analyze the continuously operated GT subsystem and periodically operated sCO_2 charging/discharging subsystem. The cost transfer associated with stored thermal energy and high-pressure CO_2 is considered, allowing the investment cost, exergy-destruction cost, and cost formation process of each component to be quantitatively evaluated.

(3) MOO is performed to reveal the relationship between thermodynamic performance and economic cost of the integrated system. System exergy efficiency and product cost are considered simultaneously to obtain the Pareto-optimal solutions. The effects of key design and operating parameters on energy conversion, heat recovery, component cost, and product cost are further analyzed, revealing the interaction between thermodynamic improvement and economic penalty in the GT-sCO$_2$ energy storage system.

The structure of the paper is outlined below. Section 2 describes the system configuration and explains its operating principles. Section 3 presents the thermodynamic models, exergy analysis, multi-period SPECO methodology, and economic models. Section 4 discusses the thermodynamic performance, exergy characteristics, and exergoeconomic cost distribution under the design condition, and introduces the MOO methodology, discusses the resulting Pareto frontier, and evaluates representative optimal solutions against the reference case. The paper concludes with the key findings in Section 5.

2. System Description and Operating Principle

2.1. System Description

A multi-period gas turbine integrated molten salt and CCES system with cascade heat utilization is proposed, as illustrated in Figure 1. The proposed system integrates continuous power generation, TES, CCES, and flexible electricity generation within a unified framework. Unlike conventional gas turbine-based combined systems, where the recovered exhaust heat is directly utilized within the same operating period, the proposed system introduces temporal decoupling between energy supply, storage, and electricity generation through independent thermal and sCO$_2$ storage processes.

The proposed system mainly consists of a GT subsystem, a molten salt TES subsystem, and a CCES subsystem. The GT subsystem adopts a conventional simple Brayton cycle consisting of a compressor (Comp2), a combustor, and a turbine (Turb2). Air drawn from the surroundings first undergoes compression before entering the combustor, where it reacts with methane. The resulting combustion products at elevated temperature subsequently expand through Turb2 to produce electricity. Residual thermal energy in the turbine exhaust is then recovered through a cascade heat utilization process.

The GT exhaust gas first enters heat exchanger (HE3), where high-temperature thermal energy is transferred to the molten salt TES system. The cold molten salt from the cold storage tank (CST) absorbs heat in HE3 and is stored in the hot storage tank (HST), completing the thermal charging process. After releasing high-grade heat in HE3, the exhaust gas enters HE4 for further low-temperature heat recovery to produce useful hot water. Therefore, the cascade heat utilization process facilitates sequential recovery of exhaust heat at different temperature levels.

The molten salt TES subsystem adopts a conventional two-tank configuration consisting of CST and HST. The stored thermal energy in HST can be released independently from the GT operating schedule. During the discharge process, the high-temperature molten salt flows through HE2 and transfers heat to the compressed CO$_2$ stream. After releasing thermal energy, the cooled molten salt returns to CST. Through this configuration, the molten salt TES provides a thermal buffer between continuous GT operation and flexible electricity generation.

The CCES subsystem consists of a low-pressure tank (LPT), a high-pressure tank (HPT), a CO$_2$ compressor (Comp1), a CO$_2$ turbine (Turb1), a recuperator (HE1), a CO$_2$-molten salt heater (HE2), a cooler, and a heat recovery unit (HE5). During the charging process, sCO$_2$ stored in LPT is pressurized by Comp1 using low-demand electricity and

subsequently stored in the HPT. In the discharging stage, pressurized CO_2 is released and first enters HE1, where it is preheated by the turbine exhaust stream. HE1 acts as an internal recuperator to recover the residual heat after expansion. The preheated CO_2 then enters HE2 and receives additional thermal input from the high-temperature molten salt stored in HST. After being heated to the required turbine inlet condition, pressurized CO_2 enters Turb1, converting its pressure energy into electrical power.

The CO_2 exhaust from Turb1 first returns to HE1 to provide heat for the incoming high-pressure CO_2 stream. The remaining thermal energy is subsequently recovered through HE5 to produce hot water. Finally, the CO_2 is cooled in the cooler to the required storage temperature before returning to the LPT for the next charging cycle. Through the coordinated utilization of sCO_2 storage and molten salt thermal storage, the proposed system achieves combined release of pressure energy and thermal energy during the discharging process.

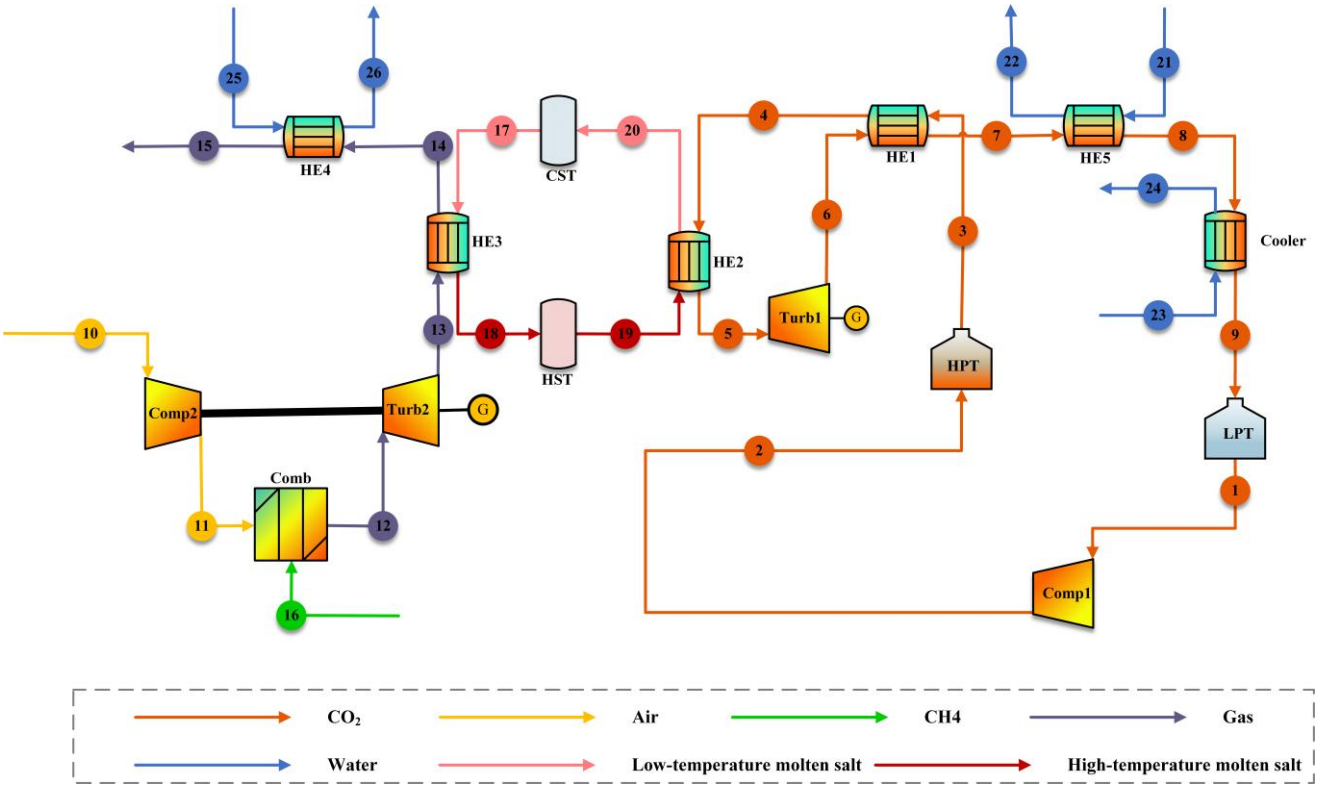


Figure 1. Schematic diagram of the proposed gas turbine integrated molten salt and CCES system.

2.2. Operating Principle

The proposed system is characterized by different operating schedules among the GT subsystem, molten salt TES subsystem, and CCES subsystem. The GT subsystem operates continuously to provide electricity and recoverable exhaust heat, whereas the CCES subsystems are scheduled according to electricity demand characteristics.

During the charging period, the GT operates continuously, and its exhaust heat is continuously recovered through HE3 and stored in the molten salt TES subsystem. Meanwhile, electricity from low-demand periods is consumed by the Comp1 to compress and store sCO_2 in the HPT. Therefore, both thermal energy storage and pressure energy storage are performed during this stage. The stored thermal energy in HST originates from GT exhaust heat, while the stored high-pressure CO_2 stores the pressure energy converted from electricity.

During the discharging period, the stored thermal energy in HST and the high-pressure CO_2 in the HPT are simultaneously utilized for electricity generation. The molten

salt provides the necessary thermal input through HE2, while the sCO_2 expands through Turb1 to produce electricity. After expansion, the remaining thermal energy of the CO_2 stream is recovered through HE1 and HE5, where internal heat recovery and hot-water production are achieved before the CO_2 is cooled and returned to the LPT.

The proposed operation strategy enables temporal decoupling among energy production, energy storage, and electricity generation. The GT can maintain continuous and stable operation, while the energy storage subsystem can respond flexibly to electricity demand variations. By combining thermal energy storage with sCO_2 storage, the proposed system provides an effective approach for improving the operational flexibility and overall energy utilization of GT-based integrated energy systems.

3. Mathematical Modeling

Comprehensive thermodynamic and economic models are developed for the proposed GT-TES-CCES system according to the operating process introduced in Section 2. The models include thermodynamic analysis, exergy analysis, exergoeconomic analysis, and MOO. Considering the different operating characteristics of the GT subsystem and the energy storage subsystems, a unified 24 h evaluation framework is adopted to consistently evaluate the continuously operated GT subsystem together with the periodically operated charging and discharging processes. Based on the established mathematical models, the energy conversion characteristics, exergy destruction, cost formation process, and thermodynamic-economic trade-off can be quantitatively analyzed. The mathematical formulation and the corresponding assumptions are presented in the following sections.

3.1. Model Assumptions

To simplify the mathematical formulation while maintaining sufficient accuracy, the following assumptions are adopted in the present study [16–18]:

1. The GT subsystem, molten salt TES subsystem, and CCES subsystem operate under quasi-steady-state conditions during each operating period. The HPT and LPT are represented as idealized storage units with prescribed pressures and inlet/outlet thermodynamic states. Transient variations in CO_2 inventory, temperature, and pressure within the storage vessels, together with the operation of pressure-compensation devices, are not explicitly modeled.
2. Changes in kinetic and potential energies, together with heat losses from pipelines and storage tanks, are neglected. The molten-salt tanks are assumed to be effectively insulated, and adiabatic storage is adopted for the daily-cycle system analysis. In practice, thermal losses would reduce the heat available for discharge and, under otherwise unchanged operating conditions without compensating heat input, could lower system efficiencies and increase the unit product exergy cost.
3. Pressure drops in pipelines, heat exchangers, and other connecting components are neglected. The electrical power consumed by the molten-salt circulation pumps and the water pumps serving the hot-water and cooling-water circuits is neglected in the present model.
4. Methane combustion in the combustor is characterized by a constant combustion efficiency of 99%. The thermophysical properties of CO_2 are obtained from REFPROP (version 9.1; National Institute of Standards and Technology, Gaithersburg, MD, USA), while those of molten salt are determined using temperature-dependent empirical correlations reported in previous studies.
5. The compressors and turbines are assumed to operate with constant isentropic efficiencies under the design operating point.

6. The GT subsystem operates continuously throughout the 24 h evaluation period, whereas the energy storage subsystem undergoes one charging process and one discharging process within each cycle. The charging and discharging durations are assumed to be equal. All thermodynamic and exergoeconomic performance indicators are evaluated based on the unified 24 h framework.
7. Sufficient external heat demand is assumed to be available to fully utilize the recovered hot water at a supply temperature of 363.15 K and a return temperature of 333.15 K during the corresponding operating periods. A site-specific heat-demand profile is not explicitly modeled.
8. A cyclic steady-state operation is assumed over each 24 h cycle, such that the thermodynamic state of the energy storage subsystem at the end of each cycle is identical to that at the beginning of the cycle.

Based on the above assumptions, the governing equations for the individual subsystems are formulated as follows.

3.2. Mathematical Modeling Framework

Following the assumptions introduced above, thermodynamic relations for the GT, TES, and CCES subsystems are formulated at the component level. A unified 24 h evaluation framework is further introduced to reconcile the different operating schedules of the continuously operated GT subsystem and the periodically operated CCES subsystem.

3.2.1. Component Models

The GT subsystem consists of an air compressor, combustor, and gas turbine. The compressor and turbine performance are determined based on the isentropic efficiency model [19]:

$$\eta_{\text{comp}} = \frac{h_{\text{out,s}} - h_{\text{in}}}{h_{\text{out}} - h_{\text{in}}} \tag{1}$$

$$\eta_{\text{turb}} = \frac{h_{\text{in}} - h_{\text{out}}}{h_{\text{in}} - h_{\text{out,s}}} \tag{2}$$

where $h_{\text{s,out}}$ is evaluated at the outlet pressure and inlet entropy, and h_{in} and h_{out} denote the inlet and outlet specific enthalpy, respectively.

The compressor power requirement and turbine power generation can be determined from Equations (3) and (4) [20]:

$$W_{\text{comp}} = \dot{m} \cdot (h_{\text{out}} - h_{\text{in}}) \tag{3}$$

$$W_{\text{turb}} = \dot{m} \cdot (h_{\text{in}} - h_{\text{out}}) \tag{4}$$

The combustor is assumed to be adiabatic, while incomplete conversion of the fuel chemical energy is accounted for through a combustion efficiency η_{cc} [21].

$$Q_{\text{fuel}} = \dot{m}_{\text{CH}_4} \cdot LHV_{\text{CH}_4} \tag{5}$$

$$\dot{m}_{16} \cdot LHV_{\text{CH}_4} \cdot \eta_{\text{cc}} + \sum(\dot{m}_{\text{in}} \cdot h_{\text{in}}) = \sum(\dot{m}_{\text{out}} \cdot h_{\text{out}}) \tag{6}$$

https://doi.org/10.3390/app162110854

where $\dot{m}_{16}$ denotes the methane flow rate (kg·s^{-1}), and LHV_{CH_4} corresponds to the methane lower heating value (kJ/kg).

For heat exchangers, the energy balance is expressed as [22]:

$$Q_{HE} = \dot{m}_h \cdot (h_{h,in} - h_{h,out}) = \dot{m}_c \cdot (h_{c,out} - h_{c,in}) \tag{7}$$

where Q indicates the heat transfer rate in kW, while $\dot{m}_h$ and $\dot{m}_c$ correspond to the hot and cold stream mass flow rates in kg·s^{-1}, the subscripts *h* and *c* are used to identify the hot and cold fluid streams, respectively.

$$\dot{Q} = UA \cdot LMTD \tag{8}$$

$$LMTD = \begin{cases} \dfrac{\Delta T_{max} - \Delta T_{min}}{In(\dfrac{\Delta T_{max}}{\Delta T_{min}})}, \dfrac{\Delta T_{max}}{\Delta T_{min}} \geq 1.7 \\ \dfrac{\Delta T_{max} + \Delta T_{min}}{2}, 1 \leq \dfrac{\Delta T_{max}}{\Delta T_{min}} < 1.7 \end{cases} \tag{9}$$

$$\begin{cases} \Delta T_{max} = \max[(T_{h,in} - T_{c,out}), (T_{h,out} - T_{c,in})] \\ \Delta T_{min} = \min[(T_{h,in} - T_{c,out}), (T_{h,out} - T_{c,in})] \end{cases} \tag{10}$$

In these relations, U denotes the overall heat transfer coefficient in kW/(m^2·K), A represents the heat transfer surface area in m^2, and LMTD denotes the logarithmic mean temperature difference. The ΔT_{max} and ΔT_{min} are defined as the temperature gaps between the hot and cold streams at the exchanger terminals, calculated based on the enthalpy differences of the respective hot and cold streams [23].

Molten salt is employed as the operating fluid and heat transfer in the TES subsystem. The thermophysical properties of molten salt are considered temperature dependent and are calculated using the correlations reported in previous studies. The sensible thermal energy stored in the molten salt is calculated as [24]:

$$Q_{molten\ salt} = \dot{m}_{molten\ salt} \int_{T_{CST}}^{T_{HST}} c_{p,molten\ salt}(T) dT \tag{11}$$

where $c_{p,molten\ salt}$ is the temperature-dependent specific heat capacity.

The CCES subsystem is modeled according to the compression, storage, expansion, and heat recovery processes of CO_2. The CO_2 compressor and turbine are modeled using the same isentropic efficiency formulation.

The prescribed-pressure representation of the HPT and LPT is a system-level idealization. In practical fixed-volume vessels, changes in CO_2 inventory and internal energy during charging and discharging cause pressure variations, which affect the compressor and turbine pressure ratios, mass flow rates, and operating conditions. Accumulator-based arrangements incorporating flexible bladders may help buffer pressure fluctuations, whereas approximately constant-pressure storage requires a suitably designed compensation mechanism. For example, flexible-membrane storage coupled with hydraulic compensation has been investigated for CO_2 energy storage [25]. The applicability of such arrangements depends on the required pressure range, temperature, storage capacity, and operating strategy.

The present study focuses on an initial system-level thermodynamic and exergoeconomic assessment under prescribed storage conditions. Transient storage

behavior and specific pressure-compensation arrangements are not explicitly modeled. Consequently, the associated regulation losses, auxiliary consumption, and additional equipment costs are excluded; these factors could reduce practical efficiency and increase the unit product exergy cost. The reported results should therefore be interpreted within these idealized storage assumptions. Future work will couple transient storage-vessel models with pressure-control strategies and off-design component characteristics to evaluate their effects on system performance and cost.

3.2.2. Energy Analysis and Unified 24 h Evaluation Framework

The instantaneous net power output during the discharge period is calculated as:

$$W_{\text{net,inst}} = W_{\text{GT,net}} + W_{\text{turb1}} \tag{12}$$

where:

$$W_{\text{GT,net}} = W_{\text{turb2}} - W_{\text{comp2}} \tag{13}$$

Considering the different operating durations of each subsystem, the performance indicators are converted into equivalent values based on a unified 24 h evaluation period.

For periodically operated components, the energy transferred during an operating period is normalized by 24 h to obtain an equivalent daily-average power. For example, the equivalent power output of the CCES turbine is defined as:

$$W_{\text{turb1,eq}} = W_{\text{turb1}} \cdot \frac{t_{\text{discharging}}}{24} \tag{14}$$

where $t_{\text{discharging}}$ is the discharge duration.

Similarly, the electricity consumption during the charging period is converted as:

$$W_{\text{comp1,eq}} = W_{\text{comp1}} \cdot \frac{t_{\text{charge}}}{24} \tag{15}$$

Therefore, the equivalent net power output is:

$$W_{\text{net,eq}} = W_{\text{GT,net}} + W_{\text{turb1,eq}} - W_{\text{comp1,eq}} \tag{16}$$

The equivalent useful heat output is calculated as:

$$Q_{\text{HW}} = Q_{\text{HE4}} + Q_{\text{HE5}} \cdot \frac{t_{\text{discharging}}}{24} \tag{17}$$

The electrical efficiency and overall energy efficiency are defined as:

$$\eta_{\text{el}} = \frac{W_{\text{net,eq}}}{Q_{\text{fuel}} + W_{\text{comp1,eq}}} \tag{18}$$

$$\eta_{\text{en}} = \frac{W_{\text{net,eq}} + Q_{\text{HW,eq}}}{Q_{\text{fuel}} + W_{\text{comp1,eq}}} \tag{19}$$

The reported system performance excludes auxiliary pumping consumption. In a practical installation, electricity is required to circulate molten salt and water through the corresponding circuits. Under otherwise unchanged operating conditions, accounting for this consumption would reduce the net electrical output and the electrical, overall energy, and exergy efficiencies. The unit product exergy cost could also increase when auxiliary consumption and pump-related costs are considered. The magnitude of these effects depends on the flow rates, hydraulic head requirements, pump efficiencies, and operating

durations of the individual circuits. Therefore, neglecting auxiliary pumping consumption introduces an optimistic bias into the performance assessment and should be recognized as a limitation of the present model.

3.2.3. Exergy Analysis

Exergy analysis is performed according to the second law of thermodynamics, with the system evaluated in terms of energy quality. For the state point j in the system, its exergy value consists of two parts: physical exergy and chemical exergy, which can be expressed as [26,27]:

$$E_{\mathrm{ph,j}} = \dot{m}_{\mathrm{j}} \cdot [h_{\mathrm{j}} - h_0 - T_0(s_{\mathrm{j}} - s_0)] \tag{20}$$

$$\dot{E}_{\mathrm{ch,j}} = \dot{n}_{\mathrm{j}} \cdot \left[\sum_K \left(y_{\mathrm{K}} \cdot e^0_{\mathrm{ch,K}} \right) + R \cdot T_0 \cdot \sum_K \left(y_{\mathrm{K}} \cdot \ln y_{\mathrm{K}} \right) \right] \tag{21}$$

where $\dot{n}_{\mathrm{j}}$ denotes molar flow rate of working fluid at state point j, y_{K} and $e^0_{\mathrm{ch,K}}$ are the mole fraction and the standard chemical exergy of component K in the mixed gas.

For each component, the exergy balance is expressed as [28]:

$$E_{\mathrm{F}} = E_{\mathrm{P}} + E_{\mathrm{D}} \tag{22}$$

where E_{F}, E_{P} and E_{D} represent the fuel exergy, product exergy, and exergy destruction, respectively.

The overall exergy efficiency is defined as [11]:

$$\eta_{ex} = \frac{E_{\mathrm{P}}}{E_{\mathrm{F}}} \tag{23}$$

All exergy-related quantities associated with periodically operated components are converted to equivalent values based on the unified 24 h evaluation framework. To ensure a consistent exergy evaluation of the proposed system, E_{F} and E_{P} of each component are defined according to the SPECO methodology [29]. The corresponding governing equations together with the fuel and product exergy definitions are summarized in Table 1. Accordingly, the E_{D} can be determined directly from the corresponding exergy balance equation [30].

Table 1. Energy balance equations and fuel/product exergy definitions for the system components.

Component	Energy Equation	Fuel Exergy	Product Exergy
Comp1	$\eta_{\mathrm{comp1}} = (h_{2,\mathrm{s}} - h_1)/(h_2 - h_1)$ $\dot{W}_{\mathrm{comp1}} = \dot{m}_1 \cdot (h_2 - h_1)$	$\dot{W}_{\mathrm{comp1}}$	$\dot{E}_2 - \dot{E}_1$
Comp2	$\eta_{\mathrm{comp2}} = (h_{11,\mathrm{s}} - h_{10})/(h_{11} - h_{10})$ $\dot{W}_{\mathrm{comp2}} = \dot{m}_{10} \cdot (h_{11} - h_{10})$	$\dot{W}_{\mathrm{comp2}}$	$\dot{E}_{11} - \dot{E}_{10}$
Turb1	$\eta_{\mathrm{turb1}} = (h_5 - h_6)/(h_5 - h_{6,s})$ $\dot{W}_{\mathrm{turb1}} = \dot{m}_5 \cdot (h_5 - h_6)$	$\dot{E}_5 - \dot{E}_6$	$\dot{W}_{\mathrm{turb1}}$
Turb2	$\eta_{\mathrm{turb2}} = (h_{12} - h_{13})/(h_{12} - h_{13,s})$ $\dot{W}_{\mathrm{turb2}} = \dot{m}_{12} \cdot (h_{12} - h_{13})$	$\dot{E}_{12} - \dot{E}_{13}$	$\dot{W}_{\mathrm{turb2}}$
Comb	$\dot{m}_{12} = \dot{m}_{11} + \dot{m}_{16}$ $\dot{m}_{11} \cdot h_{11} + \dot{m}_{16} \cdot h_{16} + \dot{m}_{16} \cdot LHV_{\mathrm{CH_4}} \cdot \eta_{\mathrm{cc}} = \dot{m}_{12} \cdot h_{12}\dot{E}_{11} + \dot{E}_{16}$ $\eta_{\mathrm{cc}} = 0.99$		$\dot{E}_{12}$

HE1	$\dot{Q}_{\mathrm{HE1}} = \dot{m}_6 \cdot (h_6 - h_7)$ $UA_{\mathrm{HE1}} = \dot{Q}_{\mathrm{HE1}} / LMTD_{\mathrm{HE1}}$	$\dot{E}_6 - \dot{E}_7$	$\dot{E}_4 - \dot{E}_3$
HE2	$\dot{Q}_{\mathrm{HE2}} = \dot{m}_4 \cdot (h_5 - h_4)$ $UA_{\mathrm{HE2}} = \dot{Q}_{\mathrm{HE2}} / LMTD_{\mathrm{HE2}}$	$\dot{E}_{19} - \dot{E}_{20}$	$\dot{E}_5 - \dot{E}_4$
HE3	$\dot{Q}_{\mathrm{HE3}} = \dot{m}_{13} \cdot (h_{13} - h_{14})$ $UA_{\mathrm{HE3}} = \dot{Q}_{\mathrm{HE3}} / LMTD_{\mathrm{HE3}}$	$\dot{E}_{13} - \dot{E}_{14}$	$\dot{E}_{18} - \dot{E}_{17}$
HE4	$\dot{Q}_{\mathrm{HE4}} = \dot{m}_{14} \cdot (h_{14} - h_{15})$ $UA_{\mathrm{HE4}} = \dot{Q}_{\mathrm{HE4}} / LMTD_{\mathrm{HE4}}$	$\dot{E}_{14} - \dot{E}_{15}$	$\dot{E}_{26} - \dot{E}_{25}$
HE5	$\dot{Q}_{\mathrm{HE5}} = \dot{m}_7 \cdot (h_7 - h_8)$ $UA_{\mathrm{HE5}} = \dot{Q}_{\mathrm{HE5}} / LMTD_{\mathrm{HE5}}$	$\dot{E}_7 - \dot{E}_8$	$\dot{E}_{22} - \dot{E}_{21}$
Cooler	$\dot{Q}_{\mathrm{Cooler}} = \dot{m}_8 \cdot (h_8 - h_9)$ $UA_{\mathrm{Cooler}} = \dot{Q}_{\mathrm{Cooler}} / LMTD_{\mathrm{Cooler}}$	$\dot{E}_8 - \dot{E}_9$	$\dot{E}_{24} - \dot{E}_{23}$
HST	$\dot{m}_{18} = \dot{m}_{19} \cdot \frac{t_{discharging}}{24}$ $h_{18} = h_{19}$	$\dot{E}_{18}$	$\dot{E}_{19} \cdot \frac{t_{discharging}}{24}$
CST	$\dot{m}_{17} = \dot{m}_{20} \cdot \frac{t_{discharging}}{24}$ $h_{17} = h_{20}$	$\dot{E}_{20} \cdot \frac{t_{discharging}}{24}$	$\dot{E}_{17}$
HPT	$\dot{m}_2 = \dot{m}_3$ $h_2 = h_3$	$\dot{E}_2$	$\dot{E}_3$
LPT	$\dot{m}_1 = \dot{m}_9$ $h_1 = h_9$	$\dot{E}_9$	$\dot{E}_1$

3.2.4. Exergoeconomic Assessment

The SPECO methodology is adopted to perform the exergoeconomic evaluation, where the unit cost of every exergy stream is obtained by combining the exergy and cost balance relationships established for each component. The SPECO method enables the identification of the economic impact of exergy destruction and provides the basis for evaluating the cost formation mechanism of the proposed GT-TES-CCES system.

The following exergy cost balance applies to each component [31]:

$$\dot{C}_{\mathrm{F,K}} + \dot{Z}_{\mathrm{K}} = \dot{C}_{\mathrm{P,K}} \tag{24}$$

where $\dot{C}_{\mathrm{F,K}}$ and $\dot{C}_{\mathrm{P,K}}$ denote the fuel and product exergy cost rates of component K, respectively, and $\dot{Z}_{\mathrm{K}}$ is the capital investment cost rate.

The cost rate corresponding to an exergy stream is determined as follows [32]:

$$\dot{C} = c \cdot \dot{E} \tag{25}$$

where c is the unit exergy cost and $\dot{E}$ is the exergy rate.

The annualized capital investment of each component is transformed into an equivalent hourly cost rate according to [33]:

$$\dot{Z}_{\mathrm{K}} = \frac{CRF \cdot PEC_{\mathrm{ref,K}} \cdot \phi}{N} \tag{26}$$

$$PEC_{\mathrm{ref,K}} = PEC_{\mathrm{original}} \cdot \frac{CEPCI_{\mathrm{ref}}}{CEPCI_{\mathrm{original}}} \tag{27}$$

where $PEC_{\mathrm{ref,K}}$ is the purchased equipment cost of component K, where is evaluated using the cost correlations listed in Table 2, where all costs are updated to the reference

year using the corresponding cost index. CRF is the capital recovery factor, $\phi = 1.06$ is the maintenance factor, and the annual operating time is assumed to be 8000 h [34].

The capital recovery factor can be evaluated using [35]:

$$CRF = \frac{i_r(1+i_r)^n}{(1+i_r)^n - 1} \tag{28}$$

where i_r denotes an interest rate of 0.1 and n = 20 years is the plant lifetime.

The cost associated with exergy destruction is calculated as:

$$\dot{C}_{D,K} = c_{F,K} \cdot \dot{E}_{D,K} \tag{29}$$

where $c_{F,K}$ is the average specific fuel exergy cost.

The unit exergy cost of the final product is obtained as [35]:

$$c_{ptot} = \frac{\dot{C}_P}{\dot{E}_P} \tag{30}$$

This quantity is adopted as a key exergoeconomic performance indicator in the subsequent analysis.

Unlike conventional GT systems, the proposed integrated system consists of continuously operated components and periodically operated charging/discharging units. Direct comparison of their cost rates would therefore lead to inconsistent exergoeconomic results.

Table 2. Purchased equipment cost correlations of major components.

Component	Cost Model	Year	CEPCI	Ref.
Comp	$\dot{m} \cdot \frac{47.1}{1-\eta_C} \cdot \pi_C \cdot In(\pi_C)$	2018	603.1	[36]
Turb	$\dot{m} \cdot \frac{392.2}{1-\eta_T} \cdot \varepsilon_T \cdot In(\varepsilon_T) \cdot (1 + e^{0.036 \cdot T_{16} - 65.66})$	2018	603.1	[36]
Combustor	$\left(\frac{46.08 \cdot \dot{m}_{16}}{0.995 - \frac{P_{out}}{P_{in}}} \right) \cdot \left(1 + e^{(0.018 T_{16} - 26.4)}\right)$	1994	368.0	[37]
HE/Cooler	$2681 \cdot A_{HE}^{0.59}$	1990	357.6	[38]
HST/CST	$4042 \cdot V_{HST}^{0.506} \cdot F_m$ [a]	2013	567.3	[39]
HPT/LPT	$1.218 \cdot f \cdot e^{11.662 - 0.6104 \cdot \ln(V_{PST}) + 0.04536 \cdot [\ln(V_{PST})]^2}$, $f = 3$	2009	521.9	[39]

[a] Material and insulation correction factor accounting for the additional costs associated with high-temperature alloys, heavy-duty thermal insulation, and nitrogen blanketing systems $(F_m = 1.8)$.

To ensure a unified evaluation basis, the investment cost rate and all exergy-related cost rates of periodically operated components are converted into equivalent values according to their actual operating durations over a 24 h cycle.

For a component operating only during the charging period:

$$\dot{Z}_{eq} = \dot{Z} \cdot \frac{t_{charge}}{24} \tag{31}$$

Similarly, for components operating only during the discharge period:

$$\dot{Z}_{\mathrm{eq}} = \dot{Z} \cdot \frac{t_{\mathrm{discharging}}}{24} \tag{32}$$

The same conversion is applied to the $\dot{C}_{\mathrm{D}}$ [40]:

$$\dot{C}_{\mathrm{D,eq}} = \dot{C}_{\mathrm{D}} \cdot \frac{t}{24} \tag{33}$$

$$f_{\mathrm{K}} = \frac{\dot{Z}_{\mathrm{K}}}{\dot{Z}_{\mathrm{K}} + \dot{C}_{\mathrm{D,K}}} \tag{34}$$

$$r_{\mathrm{K}} = \frac{c_{\mathrm{P,K}} - c_{\mathrm{F,K}}}{c_{\mathrm{F,K}}} \tag{35}$$

where t represents the corresponding operating duration, f represents the exergoeconomic factor and r represents the relative cost difference.

Following the SPECO methodology, the cost balance relations and the associated auxiliary constraints for all components are shown in Table 3.

For periodically operated components, both the investment cost rate and the exergy-related cost rates are converted into equivalent values based on the unified 24 h evaluation framework to ensure a consistent exergoeconomic evaluation.

Table 3. Cost balance equations of each component based on the SPECO methodology.

Component	Cost Rate Balance Function (Based 24 h Equivalent Quantities)	Auxiliary Equations
Comp1	$(\dot{C}_1 + \dot{C}_{\mathrm{W,Comp1}}) \cdot \frac{t_{\mathrm{discharging}}}{24} + \dot{Z}_{\mathrm{comp1}} = \dot{C}_2 \cdot \frac{t_{\mathrm{discharging}}}{24}$	$c_{\mathrm{w,comp1}} = 0.104$ \$/kWh [41]
Comp2	$\dot{C}_{10} + \dot{C}_{\mathrm{W,Comp2}} + \dot{Z}_{\mathrm{comp2}} = \dot{C}_{11}$	$c_{\mathrm{w,comp2}} = c_{\mathrm{w,turb2}}$
Turb1	$\dot{C}_5 \cdot \frac{t_{\mathrm{discharging}}}{24} + \dot{Z}_{\mathrm{turb1}} = (\dot{C}_6 + \dot{C}_{\mathrm{W,turb1}}) \cdot \frac{t_{\mathrm{discharging}}}{24}$	$c_5 = c_6$
Turb2	$\dot{C}_{12} + \dot{Z}_{\mathrm{turb2}} = \dot{C}_{13} + \dot{C}_{\mathrm{W,turb2}}$	$c_{12} = c_{13}$
Comb	$\dot{C}_{11} + \dot{C}_{16} + \dot{Z}_{Comb} = \dot{C}_{12}$	$c_{\mathrm{CH_4}} = 0.016$ \$/kWh [a] [29]
HE1	$(\dot{C}_3 + \dot{C}_6) \cdot \frac{t_{\mathrm{discharging}}}{24} + \dot{Z}_{\mathrm{HE1}} = (\dot{C}_4 + \dot{C}_7) \cdot \frac{t_{\mathrm{discharging}}}{24}$	$c_6 = c_7$
HE2	$(\dot{C}_4 + \dot{C}_{19}) \cdot \frac{t_{\mathrm{discharging}}}{24} + \dot{Z}_{\mathrm{HE2}} = (\dot{C}_5 + \dot{C}_{20}) \cdot \frac{t_{\mathrm{discharging}}}{24}$	$c_{19} = c_{20}$
HE3	$\dot{C}_{13} + \dot{C}_{17} + \dot{Z}_{\mathrm{HE3}} = \dot{C}_{14} + \dot{C}_{18}$	$c_{13} = c_{14}$
HE4	$\dot{C}_{14} + \dot{C}_{25} + \dot{Z}_{\mathrm{HE4}} = \dot{C}_{15} + \dot{C}_{26}$	$c_{14} = c_{15}, c_{25} = 0$
HE5	$(\dot{C}_7 + \dot{C}_{21}) \cdot \frac{t_{\mathrm{discharging}}}{24} + \dot{Z}_{\mathrm{HE5}} = (\dot{C}_8 + \dot{C}_{22}) \cdot \frac{t_{\mathrm{discharging}}}{24}$	$c_7 = c_8, c_{21} = 0$
Cooler	$(\dot{C}_8 + \dot{C}_{23}) \cdot \frac{t_{\mathrm{discharging}}}{24} + \dot{Z}_{\mathrm{Cooler}} = (\dot{C}_9 + \dot{C}_{24}) \cdot \frac{t_{\mathrm{discharging}}}{24}$	$c_8 = c_9, c_{23} = 0$
HST	$\dot{C}_{18} + \dot{Z}_{\mathrm{HST}} = \dot{C}_{19}$	-
CST	$\dot{C}_{20} + \dot{Z}_{\mathrm{CST}} = \dot{C}_{17}$	-
HPT	$\dot{C}_2 \cdot \frac{t_{\mathrm{discharging}}}{24} + \dot{Z}_{\mathrm{HPT}} = \dot{C}_3 \cdot \frac{t_{\mathrm{discharging}}}{24}$	-

LPT	$\dot{C}_9 \cdot \frac{t_{\text{discharging}}}{24} + \dot{Z}_{\text{LPT}} = \dot{C}_1 \cdot \frac{t_{\text{discharging}}}{24}$	-

[a] The unit cost of methane was assumed as 0.016 $/kWh, which is within the range of natural gas prices commonly adopted in exergoeconomic analyses of gas turbine-based energy systems.

The present exergoeconomic analysis and optimization use a constant reference electricity purchase price of 0.104 $/kWh for Comp1 during charging, without explicitly modeling an hourly tariff profile. For unchanged operating conditions and useful output, a lower off-peak purchase price would reduce charging expenditure and the unit product exergy cost, whereas a higher purchase price would increase them. A higher peak-period electricity selling price would increase sales revenue but would not directly change the SPECO-based production cost. Electricity sales revenue is not included in the present optimization. If time-varying tariffs are considered, charging expenditure should be evaluated using electricity-consumption-weighted purchase prices over the actual charging period.

3.3. Verification of the Proposed Model

The GT subsystem was independently simulated in Aspen Plus (version 14; Aspen Technology, Inc, Bedford, MA, USA) to verify the accuracy of the proposed thermodynamic model. As the GT subsystem functions as the core energy conversion unit of the integrated GT-TES-CCES system, its modeling accuracy directly affects the reliability of the overall system analysis.

The Aspen Plus model was established using the same boundary conditions, operating parameters, and assumptions as those adopted in the present model. The corresponding simulation flowsheet is shown in Figure 2. The air compressor, combustor, and gas turbine were modeled using appropriate Aspen Plus blocks. Specifically, the inlet temperature and pressure at state points 10 and 16, $\dot{m}_{16}$, compressor pressure ratio (PR) and T_{12} were maintained identical in both models to ensure a consistent comparison.

The validation results of the main GT parameters are summarized in Table 4. The results obtained from the developed model show good agreement with those from Aspen Plus. The deviations between the present model and the Aspen Plus results for compressor power demand, turbine power generation, and net power output remain within acceptable limits, confirming the accuracy of the proposed GT model.

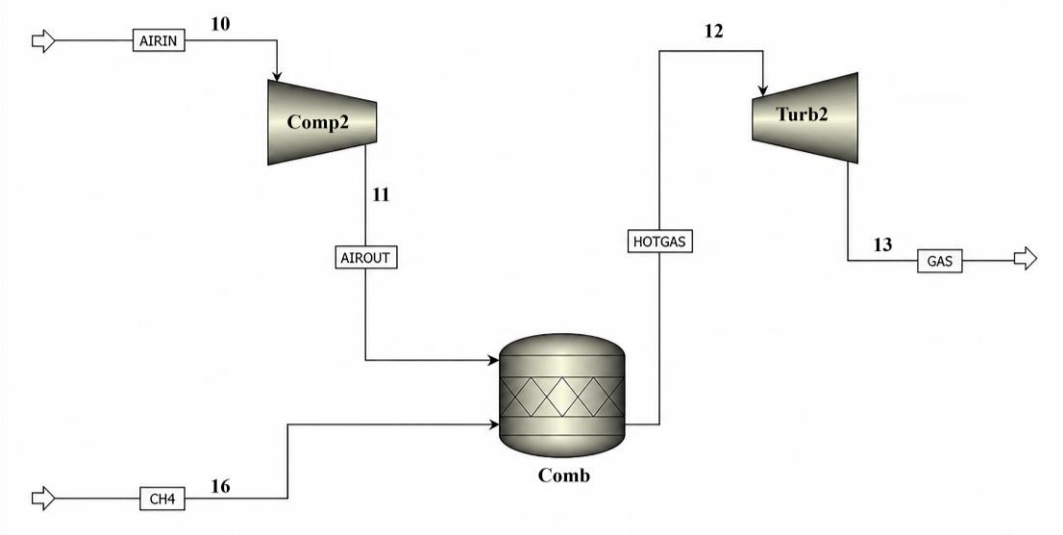


Figure 2. Aspen Plus simulation flowsheet of the GT subsystem.

https://doi.org/10.3390/app162110854

Table 4. Comparison of GT subsystem performance between the proposed model and Aspen Plus simulation.

Parameters	Unit	Present Model	Aspen Plus	Variation (–/+)	Relative Change Rate (%)
T_{11}	K	695.56	681.85	−13.71	1.97
T_{13}	K	866.40	881.27	−14.87	1.72
$\dot{m}_{10}$	kg·s^{-1}	49.55	50.99	−1.44	2.91
W_{comp2}	MW	20.36	19.30	−1.06	5.21
W_{turb2}	MW	38.11	36.70	+1.41	3.70

As shown in Table 4, the results obtained from the developed model agree well with those from Aspen Plus, with a maximum relative deviation of 5.21%. The deviations between the two models are mainly attributed to the differences in thermodynamic property evaluation and numerical calculation approaches. Nevertheless, the maximum relative deviation remains within an acceptable range, indicating that the developed GT model can reliably reproduce the thermodynamic performance of the gas turbine subsystem and provide a solid foundation for subsequent integrated system analysis.

4. Discussion and Results

This section shows the thermodynamic, exergoeconomic, and optimization results of the proposed multi-period gas turbine integrated molten salt and CCES system. Considering the different operating durations of the GT subsystem and energy storage subsystems, all performance indicators are evaluated based on the unified 24 h evaluation basis introduced in Section 3 unless otherwise specified. This approach enables a consistent comparison between the continuously operated GT subsystem and the periodically operated CCES subsystem.

The design condition and corresponding thermodynamic parameters of the main state points are first presented to establish the reference design condition. The thermodynamic performance is subsequently assessed in terms of equivalent power output, equivalent heat production, and energy efficiency. Exergy analysis is then conducted to identify the major irreversible losses and thermodynamic limitations of individual components. A multi-period exergoeconomic analysis is further performed to investigate the cost formation and transfer characteristics considering the temporal energy interaction among different subsystems. Finally, sensitivity analysis and MOO are applied to quantify the effects of key parameters and identify Pareto-optimal solutions balancing thermodynamic performance and product cost.

4.1. Thermodynamic Performance Under Design Conditions

The main design parameters and boundary conditions are listed in Table 5. The GT subsystem is operated under a fixed PR and turbine inlet temperature (TIT), while the η_{comp2} and η_{turb2} are selected based on typical values of industrial gas turbines. For the CCES subsystem, the operating pressures, turbine inlet conditions, and component efficiencies are specified according to representative parameters reported in previous studies. The molten salt TES subsystem is designed to recover high-temperature exhaust heat from the GT subsystem and provide thermal input during the sCO_2 discharge process.

Table 5. Design parameters and boundary conditions of the proposed system.

Parameters	Value
Ambient temperature (K)	298.15
Ambient pressure (kPa)	101.3
Isentropic efficiency of the Comp1 (%)	89.0
Isentropic efficiency of the Turb1 (%)	90.0
Isentropic efficiency of the Comp2 (%)	85.0
Isentropic efficiency of the Turb2 (%)	88.0
terminal temperature difference of heat exchangers (K)	10.0
terminal temperature difference of Cooler (K)	10.0
Pressure of LPT (MPa)	8.0
Pressure of HPT (MPa)	27.0
Charge/Discharge time (h)	8.0
Mass flow of CH_4 ($kg \cdot s^{-1}$)	1.0
Pressure ratio of Comp2	15.0
Inlet temperature of Turb2 (K)	1473.15
Pressure drops of Combustion (%)	4
Combustion chamber combustion efficiency (%)	99.0
Inlet water temperature (K)	333.15
Outlet water temperature (K)	363.15

The thermodynamic parameters of the main state points are listed in Table 6. These results provide the basic thermodynamic information for subsequent energy, exergy, and exergoeconomic analyses. The temperature, pressure, enthalpy, entropy, and mass flow rate of each working stream are calculated based on the thermodynamic models described in Section 3.

Table 6. Thermodynamic parameters of the main state points.

State Points	T /K	P /MPa	M /kg·s^{-1}	H /kJ·kg^{-1}	S /kJ·(kg·K)$^{-1}$	Working Fluid
1	308.15	8.0	143.29	352.29	1.49	CO_2
2	369.54	27.0	143.29	390.82	1.51	CO_2
3	369.54	27.0	143.29	390.82	1.51	CO_2
4	523.15	27.0	143.29	648.56	2.10	CO_2
5	828.15	27.0	143.29	1036.88	2.68	CO_2
6	683.86	8.0	143.29	879.80	2.71	CO_2
7	457.72	8.0	143.29	622.06	2.25	CO_2
8	373.15	8.0	143.29	519.90	2.01	CO_2
9	308.15	8.0	143.29	352.29	1.49	CO_2
10	298.15	0.10	49.55	298.45	6.86	Air
11	695.56	1.52	49.55	709.27	6.95	Air
12	1473.15	1.46	50.55	1795.94	7.82	Gas
13	866.40	0.10	50.55	1042.11	7.95	Gas
14	543.15	0.10	50.55	675.23	7.42	Gas
15	373.15	0.10	50.55	492.30	7.02	Gas
16	298.15	1.52	1.0	895.97	5.24	CH_4
17	533.15	0.10	38.96	355.91	0.88	Molten Salt
18	838.15	0.10	38.96	831.99	1.58	Molten Salt
19	838.15	0.10	116.87	831.99	1.58	Molten Salt
20	533.15	0.10	116.87	355.91	0.88	Molten Salt
21	333.15	0.10	116.35	251.25	0.83	Water
22	363.15	0.10	116.35	377.06	1.19	Water

23	298.15	0.10	718.17	104.92	0.37	Water
24	306.15	0.10	718.17	138.36	0.48	Water
25	333.15	0.10	73.50	251.25	0.83	Water
26	363.15	0.10	73.50	377.06	1.19	Water

The key performance indicators are summarized in Table 7. Since the GT subsystem and energy storage subsystems operate over different time periods, all reported power and heat production values are expressed as equivalent values based on the unified 24 h evaluation period.

Under the design condition, the proposed system achieves η_{el} of 48.71%, η_{en} of 75.97%, and η_{ex} of 50.29%. The $W_{net,eq}$ and Q_{HW} are 23.41 MW and 14.13 MW, respectively, while the c_{ptot} is 14.32 \$·GJ^{-1}. During the discharge period, the $W_{net,inst}$ reaches 40.26 MW, demonstrating the capability of the proposed system to shift electricity generation from low-demand periods to peak-demand periods.

Table 7. Overall performance indicators of the proposed system under the design condition.

Parameters	Value
η_{el}	48.71%
η_{en}	75.97%
η_{ex}	50.29%
$W_{net,inst}$ (MW)	40.26
$W_{net,eq}$ (MW)	23.41
Q_{HW} (MW)	14.13
c_{ptot} (\$·GJ^{-1})	14.32

The GT subsystem serves as the primary energy conversion unit and provides continuous electricity generation throughout the operating period. However, a significant amount of thermal energy remains available in the GT exhaust gas because of the limited conversion efficiency of the Brayton cycle. Through the integration of molten salt TES, the high-temperature exhaust heat is recovered and stored for subsequent utilization during the CO_2 discharge process. Meanwhile, the remaining low-temperature exhaust heat is further recovered for hot water production through the cascade heat utilization process.

The CCES subsystem provides additional electricity generation capability during high-demand periods by converting stored pressure energy into electrical output. During the charging period, electricity consumption is shifted to low-demand periods, while the stored high-pressure CO_2 is released during the discharge period. Because the CO_2 expansion process requires additional thermal input, the molten salt TES subsystem provides the necessary heat source and improves the utilization of recovered GT exhaust energy.

The combined utilization of molten salt thermal storage and sCO_2 storage enables temporal decoupling between continuous energy supply and flexible electricity generation. Compared with conventional GT systems without energy storage, the proposed configuration improves the utilization of exhaust heat while providing additional electricity and useful heat outputs.

The recovered hot water, supplied at 90 °C with a return temperature of 60 °C, is intended for potential district or campus heating applications. It may also provide heat for domestic hot-water preparation through secondary heat exchangers. These applications require external heat demand compatible with the available temperatures, heat output, and operating periods. Site-specific demand matching is not explicitly modeled in the present study.

The reported performance assumes full utilization of the recovered heat. This requires an external demand capable of accepting the continuous heat output from HE4 and the additional heat output from HE5 during discharge. Without sufficient demand, unused heat should be excluded from the useful thermal output and product exergy. Consequently, the overall energy and exergy efficiencies would decrease under otherwise unchanged operating conditions, and the SPECO assessment would need to reflect the actual useful products. The reported combined power-and-heat performance should therefore be interpreted as conditional on adequate heat utilization.

However, energy-based indicators cannot fully reflect the quality degradation of different energy streams or identify the irreversible losses associated with each component. Therefore, an exergy analysis is conducted in the following section to evaluate the thermodynamic limitations.

4.2. Exergy Analysis and Destruction Characteristics

Exergy analysis is performed to identify the thermodynamic limitations of GT-CCES integrated system by evaluating the irreversible losses associated with different energy conversion processes. Compared with energy analysis, exergy analysis considers both the quantity and quality of energy and therefore provides a more comprehensive assessment of the system performance. The $\dot{E}_{\mathrm{F}}$, $\dot{E}_{\mathrm{P}}$, $\dot{E}_{\mathrm{D}}$, and η_{ex} of each component are calculated according to the SPECO methodology presented in Section 3. All exergy-related quantities are evaluated on the unified 24 h basis. The corresponding results are summarized in Table 8, while the component exergy efficiencies are shown in Figure 3.

In Table 8 and Figure 3, the mechanical components, including the Comp2, Comp1, Turb2, and Turb1, all exhibit exergy efficiencies higher than 90%, indicating relatively limited irreversible losses during the compression and expansion processes. In contrast, the combustor shows the largest exergy destruction and the lowest exergy efficiency among the major energy conversion components. This is mainly attributed to the inherent irreversibility of fuel combustion and the large temperature difference involved in the combustion process.

The heat exchangers exhibit different exergy characteristics depending on their operating temperature levels. HE2 and HE3 achieve exergy efficiencies of 98.49% and 97.85%, respectively, owing to the favorable temperature matching between the hot and cold streams. By comparison, HE1 has a relatively large exergy destruction because of the significant heat transfer between the two CO_2 streams. HE4 and HE5 show lower exergy efficiencies since they recover low-grade thermal energy for hot-water production, where the available work potential is inherently limited.

The cooler exhibits the lowest exergy efficiency because the remaining low-grade thermal energy of the expanded sCO_2 is rejected before the working fluid returns to the low-pressure storage tank. In contrast, the HST, CST, HPT, and LPT exhibit exergy efficiencies approaching 100%, as ideal adiabatic storage is assumed and storage losses are neglected in the present model.

Overall, the results indicate that the major thermodynamic losses originate from combustion, recuperative heat transfer, and low-temperature heat rejection. Although the integration of molten salt TES and sCO_2 storage cannot eliminate these irreversible losses, it effectively transfers high-temperature exhaust heat across different operating periods and improves the utilization of available energy. The thermodynamic characteristics identified here provide the basis for the subsequent multi-period exergoeconomic analysis.

Table 8. Exergy destruction and exergy efficiency of the main components.

Components	$\dot{E}_{F,k}$ /MW	$\dot{E}_{P,k}$ /MW	$\dot{E}_{D,k}$ /MW	ε_k /%
Comp1	5.52	5.03	0.49	91.10
Comp2	20.36	18.99	1.37	93.29
Turb1	23.61	22.51	1.10	95.33
Turb2	40.00	38.11	1.89	95.29
Comb	71.39	55.24	16.15	77.38
HE1	17.40	11.65	5.75	66.96
HE2	31.07	30.60	0.47	98.49
HE3	10.58	10.36	0.23	97.85
HE4	3.16	1.32	1.84	41.83
HE5	4.07	2.10	1.97	51.48
Cooler	2.20	0.32	1.88	14.41
HST	14.01	14.01	0	100
CST	3.65	3.65	0	100
HPT	36.10	36.10	0	100
LPT	31.07	31.07	0	100

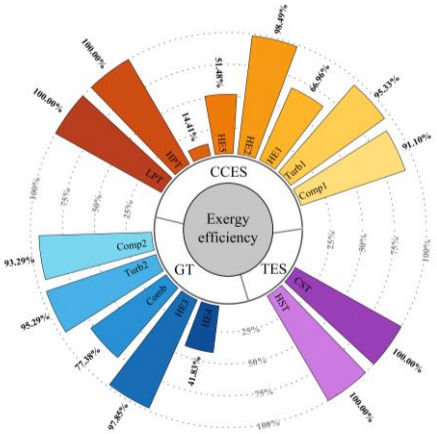


Figure 3. Component-level exergy efficiency characteristics of the proposed GT–TES–CCES system.

4.3. Multi-Period Exergoeconomic Analysis

The exergoeconomic performance of the proposed system is evaluated using the multi-period SPECO methodology developed in Section 3. The $\dot{Z}$, $\dot{C}_D$, $\dot{Z}+\dot{C}_D$, f, and r of each component are listed in Table 9, while the distribution of the capital cost rates among different subsystems and components is shown in Figure 4.

Table 9. Exergoeconomic performance of the main components under the design condition.

Component	$\dot{Z}$ $\$\cdot h^{-1}$	$\dot{C}_D$ $\$\cdot h^{-1}$	$\dot{Z}+\dot{C}_D$ $\$\cdot h^{-1}$	f %	r %
Comp1	5.20	17.03	22.23	23.39	12.75
Comp2	13.05	43.83	56.88	22.94	9.34
Turb1	47.63	23.57	71.20	66.90	14.80
Turb2	131.01	51.47	182.48	71.80	17.54
Comb	4.78	339.98	344.77	1.39	29.65
HE1	20.24	122.88	143.12	14.14	57.47
HE2	82.95	5.09	88.04	94.22	26.61

HE3	31.11	6.20	37.30	83.39	13.20
HE4	6.93	50.24	57.16	12.12	158.24
HE5	12.69	42.22	54.91	23.11	122.59
Cooler	3.20	40.21	43.41	7.38	641.50
HST	8.20	0	8.20	100	1.84
CST	7.73	0	7.73	100	6.52
HPT	1.38	0	1.38	100	0.16
LPT	1.70	0	1.70	100	0.26

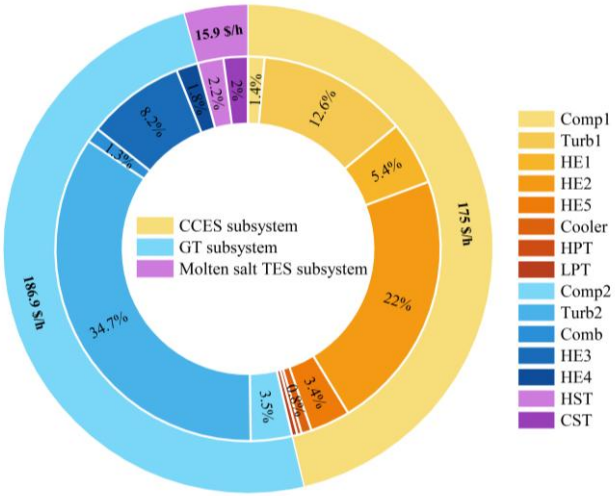


Figure 4. Distribution of capital cost rates among different subsystems and components.

As shown in Figure 4, the GT subsystem and the CCES subsystem dominate the total capital investment, contributing approximately 49.5% and 46.3%, respectively, whereas the molten salt TES subsystem accounts for only 4.2%. Within the GT subsystem, Turb2 exhibits the highest capital cost rate, followed by HE3. In the CCES subsystem, HE2 and Turb1 represent the major investment components. This distribution indicates that the overall capital cost is primarily associated with turbomachinery and high-temperature heat exchangers, while the additional investment required for the molten salt TES subsystem is relatively limited.

The exergoeconomic results further reveal that the components with the highest capital cost are not necessarily those with the highest exergy destruction cost. As listed in Table 9, the combustor exhibits the largest exergy destruction cost rate but a relatively low capital cost rate, resulting in an exergoeconomic factor of only 1.39%. This indicates that the economic penalty of the combustor is mainly caused by thermodynamic irreversibility rather than equipment investment. In contrast, HE2 has a relatively small exergy destruction cost rate but a high capital cost rate, corresponding to the highest exergoeconomic factor among the heat exchangers. Therefore, the economic performance of HE2 is mainly governed by equipment investment, suggesting that reducing heat-transfer area or improving heat exchanger design would be more effective than further reducing exergy destruction.

The heat recovery components exhibit different exergoeconomic characteristics. Although HE3 has a relatively high exergoeconomic factor, indicating that its total cost is mainly dominated by investment, HE4, HE5, and the Cooler present relatively low exergoeconomic factors and considerably larger relative cost differences. In particular, the Cooler exhibits the highest relative cost difference, followed by HE4 and HE5. This behavior is mainly attributed to the recovery or rejection of low-grade thermal energy,

where the available exergy decreases significantly during the heat transfer process, leading to a substantial increase in the unit exergy cost despite their relatively low capital investment.

For the storage units, the HST, CST, HPT, and LPT are modeled under idealized loss-free storage assumptions; therefore, no internal exergy destruction is considered, and their exergoeconomic factors reach 100%. Their relatively small capital cost rates further indicate that the additional investment associated with thermal and pressure energy storage is limited compared with the major energy conversion components.

These results clearly demonstrate that exergy analysis alone is insufficient to identify the priority components for system improvement, highlighting the necessity of the proposed multi-period exergoeconomic analysis. Overall, the multi-period SPECO analysis demonstrates that the product cost is jointly determined by equipment investment and exergy destruction. While the GT turbines and high-temperature heat exchangers dominate the capital investment, the combustor remains the major contributor to exergy destruction cost. These results indicate that different components require different optimization strategies and provide the economic basis for the subsequent sensitivity analysis and MOO.

4.4. Sensitivity Analysis

To further evaluate the influence of key design and operating parameters on the proposed system, a sensitivity analysis is conducted under the design condition. Six representative parameters, including the PR, TIT, P_{HPT}, charging time, η_{turb1}, and η_{turb2}, are individually varied while keeping the remaining parameters unchanged. Six performance indicators, namely the η_{el}, η_{en}, η_{ex}, $W_{net,inst}$, Q_{HW}, and c_{ptot}, are adopted to evaluate the thermodynamic and economic responses. The obtained results provide the basis for selecting the decision variables used in the subsequent multi-objective optimization.

4.4.1. Effect of PR

Figure 5 illustrates the effects of PR. As PR increases from 10 to 20, both η_{el} and η_{ex} increase continuously, indicating that a higher-pressure ratio improves the energy conversion capability and enhances the overall exergy utilization of the integrated system.

https://doi.org/10.3390/app162110854

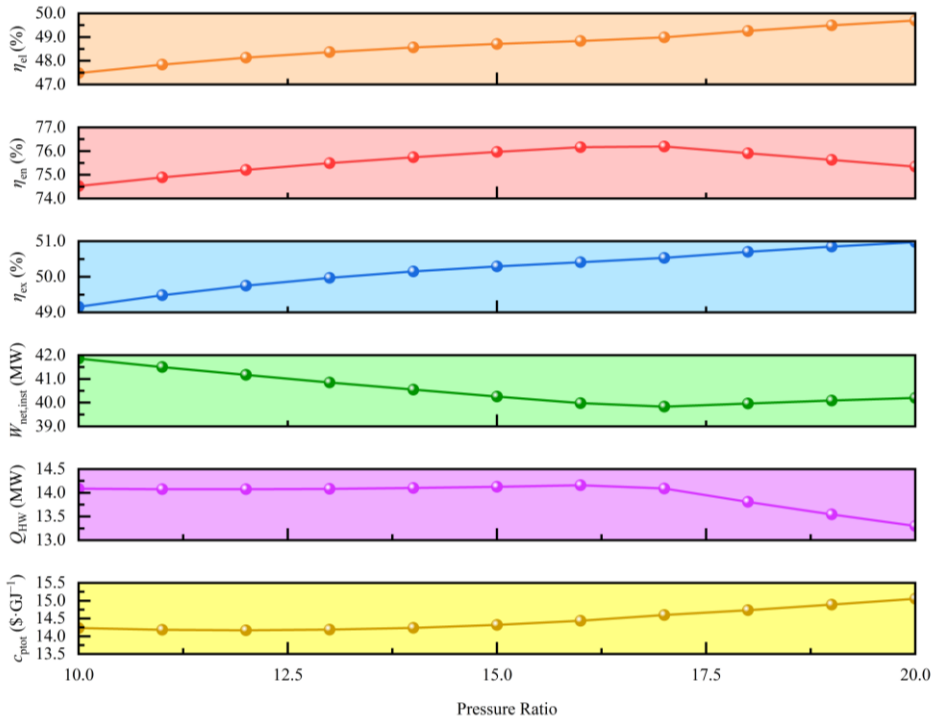


Figure 5. Effects of PR on the thermodynamic and economic performance of the proposed system.

In contrast, η_{en} first increases and then decreases slightly, reaching its maximum value at a PR of approximately 16–17. This trend results from the reduction in GT exhaust temperature at higher pressure ratios, which decreases the amount of recoverable heat available for the molten salt TES and subsequent hot-water production. Consequently, the Q_{HW} remains nearly constant at low PR values but gradually declines when PR exceeds the design condition. Meanwhile, $W_{net,inst}$ decreases slightly before exhibiting a marginal recovery at higher pressure ratios.

The c_{ptot} shows a slight decrease at low PR values, followed by a continuous increase as PR further increases. Although a higher-pressure ratio improves the thermodynamic performance, the associated increase in equipment cost and the reduction in heat recovery weaken the overall economic benefit. Therefore, an excessively high-pressure ratio is not desirable, and an intermediate PR provides a more balanced compromise between thermodynamic performance and economic cost.

4.4.2. Effect of Inlet Temperature of Gas Turbine

Figure 6 presents the effects of TIT. As TIT increases, η_{el} and η_{ex} increase continuously, indicating that a higher turbine inlet temperature enhances the Brayton cycle performance and improves the overall utilization of the supplied fuel exergy.

The η_{en} increases rapidly at relatively low TIT values and then remains nearly constant. The higher TIT also raises the GT exhaust temperature, providing more recoverable thermal energy for the molten salt TES subsystem. Consequently, $W_{net,inst}$ decreases slightly at lower TIT values and then increases above approximately 1175 °C. Q_{HW} first increases and reaches its maximum at approximately 1175 °C, after which it gradually decreases. This behavior indicates that, although higher TIT provides more exhaust heat, a larger proportion of the available energy is converted into electricity, reducing the fraction finally recovered as useful heat.

The c_{ptot} decreases noticeably as TIT increases and approaches a nearly constant value at high TIT. The improvement in thermodynamic performance offsets the increase in equipment cost, resulting in a lower unit product cost. Therefore, increasing TIT is

generally beneficial to both the thermodynamic and economic performance, although excessively high turbine inlet temperatures may impose more stringent material and operational requirements in practical applications.

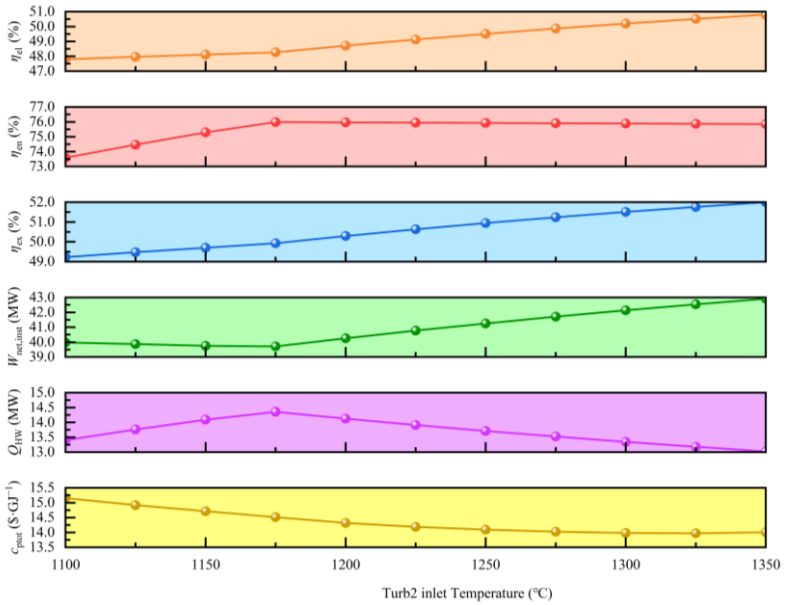


Figure 6. Effects of TIT on the thermodynamic and economic performance of the proposed system.

4.4.3. Effect of Charging Pressure

Figure 7 illustrates the effects of the HPT pressure. As the HPT pressure increases from 22 to 32 MPa, the η_{el}, η_{en}, and η_{ex} all increase gradually. A higher storage pressure increases the pressure ratio of the CO_2 expansion process, allowing more pressure energy stored during the charging stage to be converted into useful work during discharge.

The increase in storage pressure also leads to a continuous improvement in the $W_{net,inst,}$ whereas the Q_{HW} decreases slightly. This is because a larger fraction of the available energy is converted into electricity through the CO_2 turbine, leaving less residual thermal energy available for subsequent heat recovery.

The c_{ptot} exhibits a slight upward trend with increasing HPT pressure. Although the thermodynamic performance is improved, the higher operating pressure requires more expensive compression and high-pressure storage equipment, resulting in a moderate increase in product cost. Therefore, increasing the HPT pressure enhances the electricity generation capability and overall system efficiency, while a trade-off exists between the thermodynamic improvement and the associated economic penalty.

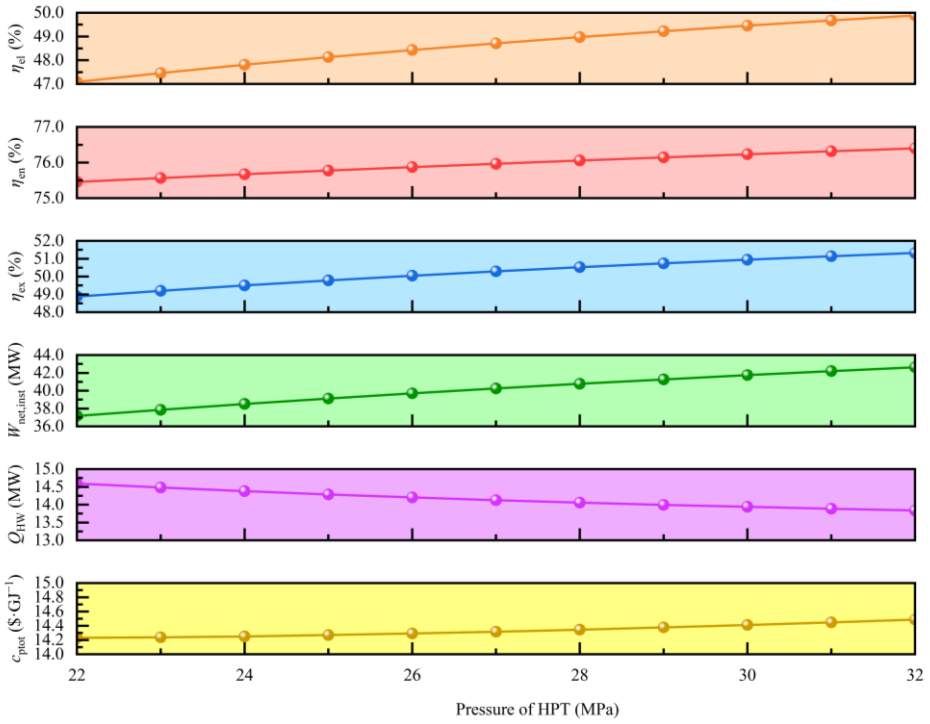


Figure 7. Effects of HPT pressure on the thermodynamic and economic performance of the proposed system.

4.4.4. Effect of Charge/Discharge Time

Figure 8 illustrates the effects of the charge/discharge time. As the charge/discharge time increases from 2 h to 12 h, the η_{el}, η_{en}, and η_{ex} remain nearly unchanged. Since the operating conditions of both the GT and CO_2 cycles are fixed, varying the operating duration only changes the daily operating schedule rather than the thermodynamic characteristics of the system.

The Q_{HW} also remains almost constant because it is evaluated on the unified 24 h basis. In contrast, the $W_{net,inst}$ decreases significantly with increasing charge/discharge time. A longer discharge duration distributes the stored energy over a longer operating period, thereby reducing the average power generation rate during electricity release.

The c_{ptot} decreases continuously as the charge/discharge time increases. Extending the operating duration improves the utilization of the installed equipment and reduces the capital cost allocated to each unit of useful product. Therefore, although the charge/discharge time has little influence on the thermodynamic efficiencies, it considerably affects the power output characteristics and the overall economic performance of the proposed system.

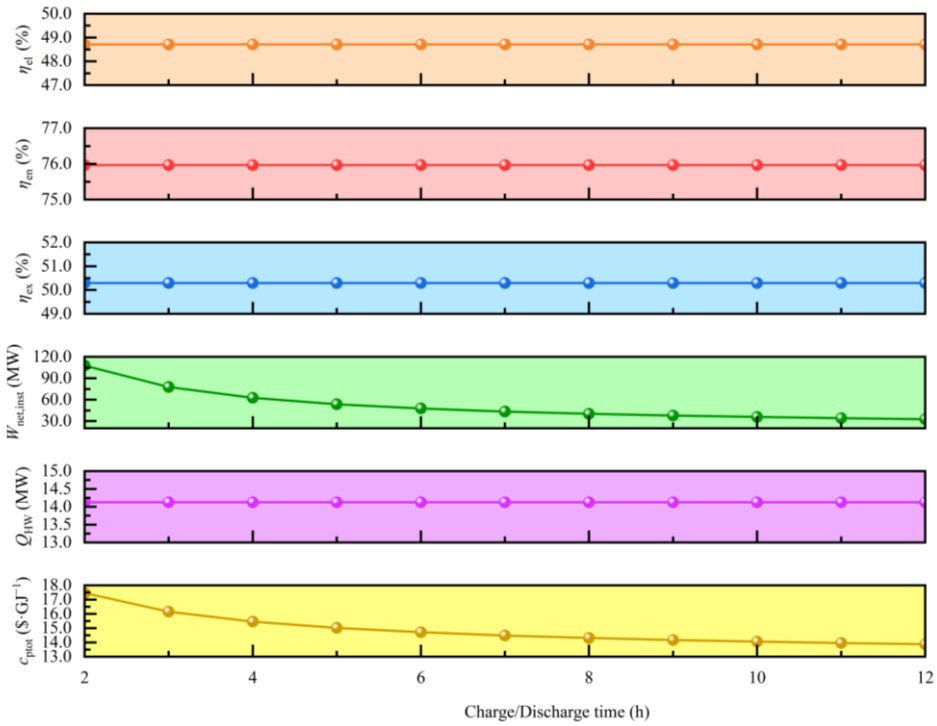


Figure 8. Effects of Charge/Discharge time on the thermodynamic and economic performance of the proposed system.

4.4.5. Effect of CO_2 Turbine Efficiency

Figure 9 presents the effects of the η_{turb1}. As the isentropic efficiency of the CO_2 turbine increases from 0.82 to 0.92, both the η_{el} and η_{ex} increase continuously. A higher turbine efficiency reduces the irreversibility during the CO_2 expansion process, allowing more of the stored pressure energy to be converted into useful electrical power.

$W_{net,inst}$ also increases gradually with increasing turbine efficiency, whereas Q_{HW} decreases slightly. This is because a more efficient expansion extracts additional work from the CO_2 stream, resulting in a lower exhaust temperature and consequently less recoverable thermal energy for hot-water production. In contrast, η_{en} remains nearly constant, indicating that the improvement in electricity generation is largely offset by the reduction in useful heat output.

The c_{ptot} decreases slightly to a minimum near an isentropic efficiency of 0.89–0.90 and then increases marginally. The enhanced thermodynamic performance compensates for the additional equipment cost associated with higher turbine efficiency. Therefore, improving the CO_2 turbine performance is beneficial for enhancing electricity generation and exergy utilization while maintaining a relatively stable economic performance.

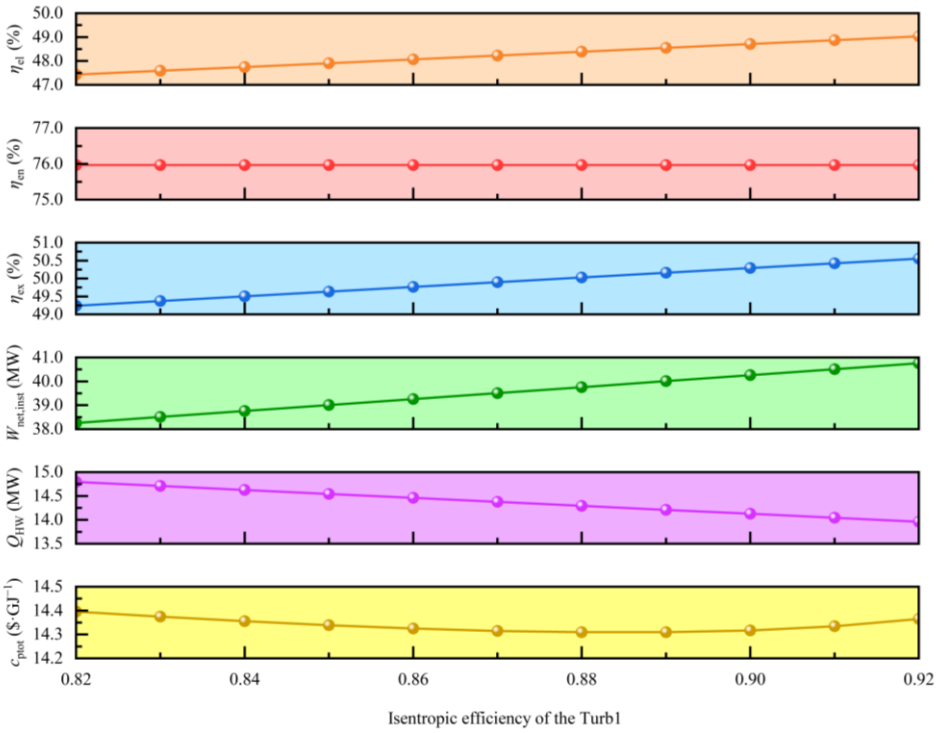


Figure 9. Effects of η_{turb1} on the thermodynamic and economic performance of the proposed system.

4.4.6. Effect of Gas Turbine Efficiency

Figure 10 illustrates the influence of the η_{turb2}. As the isentropic efficiency of the gas turbine increases from 0.82 to 0.92, the η_{el}, η_{en} and η_{ex} all increase almost linearly. The higher turbine efficiency enables more effective conversion of the combustion gas exergy into useful work, thereby improving the overall thermodynamic performance.

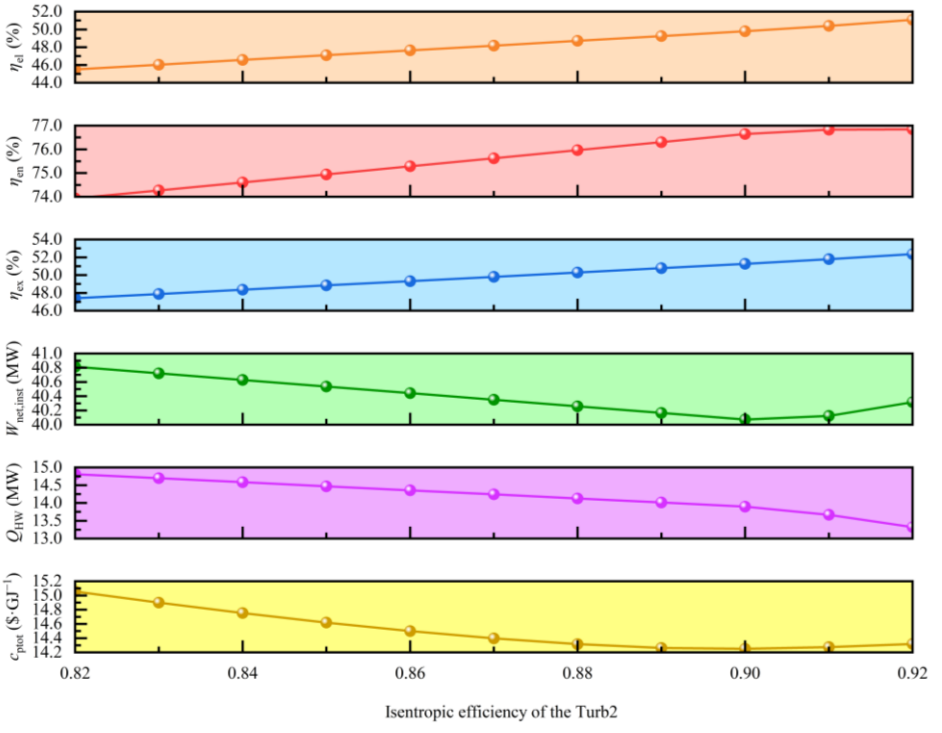


Figure 10. Effects of η_{turb2} on the thermodynamic and economic performance of the proposed system.

Q_{HW} decreases gradually with increasing turbine efficiency because the GT exhaust temperature is reduced after more expansion work is extracted, leaving less recoverable waste heat for the molten salt TES and hot-water production. $W_{net,inst}$ exhibits only a slight variation over the investigated range, indicating that the GT turbine efficiency mainly affects the continuous GT subsystem, while the discharge power is dominated by the CO_2 expansion process.

The c_{ptot} decreases with increasing turbine efficiency and reaches a minimum around 0.89–0.90, after which only a slight increase is observed. This indicates that the thermodynamic benefits obtained from improving the GT turbine efficiency gradually diminish at higher efficiency levels. Therefore, selecting an excessively high turbine efficiency may not provide significant additional economic advantages.

4.5. Multi-Objective Optimization

4.5.1. Optimization Problem Formulation

The sensitivity analysis presented in Section 4.4 indicates that several design parameters have significant influences on the thermodynamic and economic performance of the proposed system. To further determine the optimal operating conditions while balancing thermodynamic performance and economic cost, a MOO is performed.

Based on the sensitivity analysis, six design variables are selected as the optimization variables, including PR, TIT, the pressure of HPT, Charge/Discharge time, η_{turb1}, and η_{turb2}. The corresponding ranges are summarized in Table 10.

Table 10. Optimization variables and ranges for the multi-objective optimization of the proposed system.

Variable	Unit	Lower Limit	Upper Limit
PR	-	10	20
TIT	K	1373.15	1673.15
P_{HPT}	MPa	22	32
Charge/Discharge time	h	4	12
η_{turb1}	%	82.0	92.0
η_{turb2}	%	82.0	92.0

The optimization simultaneously maximizes η_{ex} and minimizes c_{ptot}. Therefore, the optimization problem can be expressed as:

$$\begin{cases} \max & \eta_{ex} \\ \min & c_{ptot} \end{cases} \tag{36}$$

The decision-variable vector is defined as:

$$X = \left[PR, \mathrm{TIT}, P_{\mathrm{HPT}}, t_{\text{charge/discharge time}}, \eta_{\mathrm{turb1}}, \eta_{\mathrm{turb2}} \right]^{\mathrm{T}} \tag{37}$$

where each design variable is constrained within its predefined operating range. The thermodynamic and exergoeconomic evaluations follow the governing equations and assumptions presented in Section 3. No additional performance constraints, such as minimum electrical power output or minimum hot-water production, are imposed.

MOO is performed using the Non-dominated Sorting Genetic Algorithm II (NSGA-II), owing to its strong global search capability and its effectiveness in producing a diverse set of Pareto-optimal solutions [42]. The algorithm was configured with a population size of 300 and run for 300 generations.

4.5.2. Pareto Optimal Solutions

The Pareto-optimal solutions obtained using the NSGA-II algorithm are illustrated in Figure 11, where the η_{ex} is maximized while the c_{ptot} is minimized simultaneously. As expected, the two objectives exhibit a clear trade-off relationship. Improving the exergy efficiency generally results in an increase in the product unit exergy cost, indicating that further thermodynamic improvement requires additional investment and higher-quality energy conversion components.

The Pareto front can be divided into three characteristic regions. In the left region (A–B), the product unit exergy cost remains low, whereas the exergy efficiency is relatively limited. In the middle region (C–D), the increase in exergy efficiency is accompanied by only a moderate increase in the unit cost, representing a favorable compromise between thermodynamic and economic performance. In contrast, the right region (E–F) provides only marginal improvements in exergy efficiency at the expense of a significant increase in the product unit exergy cost, indicating diminishing economic returns.

To determine the final operating condition, TOPSIS is employed to select a compromise solution from the Pareto front. Exergy efficiency and unit product exergy cost are used as the two decision criteria, with equal weights of 0.5. Exergy efficiency is treated as a benefit criterion, whereas unit product exergy cost is treated as a cost criterion. The criteria are normalized using min–max normalization, with both normalized values defined such that lower values indicate better performance:

$$\eta_{ex,i}^{*} = \frac{\eta_{ex,max} - \eta_{ex,i}}{\eta_{ex,max} - \eta_{ex,min}} \tag{38}$$

$$c_{ptot,i}^{*} = \frac{c_{ptot,i} - c_{ptot,min}}{c_{ptot,max} - c_{ptot,min}} \tag{39}$$

where i denotes a candidate solution, and the subscripts max and min denote the maximum and minimum values of each criterion among the non-dominated solutions obtained by NSGA-II.

Accordingly, the positive and negative ideal points in the normalized space are (0,0) and (1,1), respectively. Under equal weighting, the common weight factor cancels in the closeness coefficient, and the Euclidean distances to the two ideal points can be expressed as:

$$d_i^{-} = \sqrt{(1-\eta_{ex,i}^{*})^2 + (1-c_{ptot,i}^{*})^2} \tag{40}$$

$$d_i^{+} = \sqrt{(0-\eta_{ex,i}^{*})^2 + (0-c_{ptot,i}^{*})^2} \tag{41}$$

The relative closeness coefficient is calculated as:

$$CC_i = \frac{d_i^{-}}{d_i^{+} + d_i^{-}} \tag{42}$$

The candidate with the highest CC_i is selected as the final compromise solution. The selected solution is indicated by the orange star at (54.82, 13.55) in Figure 11 and represents a balance between exergy efficiency and unit product exergy cost under the specified equal weights. The red star denotes the positive ideal reference point (55.95, 13.26) in the original objective space, corresponding to (0,0) in the normalized space. The corresponding design variables and system performance are presented in the following section.

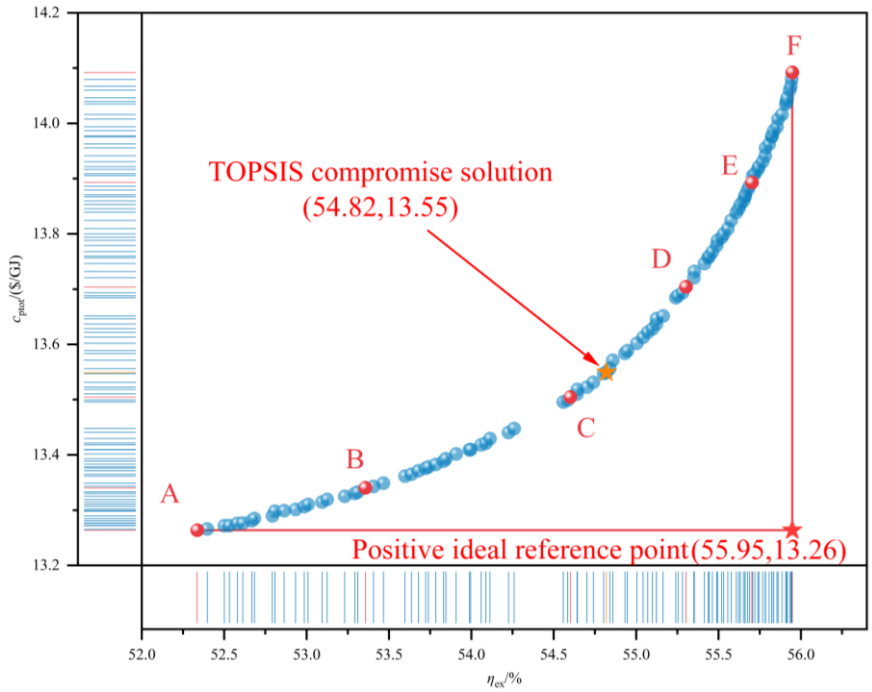


Figure 11. Pareto-optimal solutions obtained by NSGA-II for maximizing exergy efficiency and minimizing product unit exergy cost.

4.5.3. Optimal Solution and Performance Comparison

The optimal operating conditions selected from the Pareto front and the corresponding system performance are listed in Table 11. Compared with the baseline design, the optimized configuration exhibits noticeable changes in several operating parameters. Specifically, the HPT pressure increases from 27.0 MPa to 30.32 MPa, while the charging/discharging time is extended from 8.0 h to 11.97 h. Meanwhile, the η_{turb1} and η_{turb2} are improved to 91.96% and 91.99%, respectively. In contrast, the PR remains almost unchanged, whereas the GT turbine inlet temperature is increased from 1473.15 K to 1629.31 K.

The optimized operating conditions lead to significant improvements in system efficiencies and unit product exergy cost. The η_{el} increases from 48.71% to 53.99%, while the η_{ex} rises from 50.29% to 54.82%. In addition, the η_{en} is slightly improved from 75.97% to 77.37%. From the economic perspective, the c_{ptot} decreases from 14.32 to 13.55 \$·GJ^{-1}, corresponding to a reduction of approximately 5.38%. These results indicate that the optimized design enhances overall exergy utilization while simultaneously reducing the unit product exergy cost.

It should be noted that the $W_{net,inst}$ decreases from 40.26 MW to 36.55 MW, and the Q_{HW} decreases from 14.13 MW to 12.19 MW after optimization. This optimization prioritizes maximizing the η_{ex} and minimizing the c_{ptot}, rather than maximizing the peak power output or heat production. Power output and hot-water production contribute to the system exergy and cost balances but are not included as separate TOPSIS criteria. No minimum electrical power output or hot-water production requirements are imposed. Since exergy efficiency and unit product exergy cost are ratio-based indicators, their improvement does not necessarily imply an increase in absolute output. The reductions in instantaneous net power and heat output are therefore accepted trade-offs of the selected solution.

The distinction between instantaneous power and daily energy output should also be emphasized. The $W_{net,inst}$ represents net power during the discharge period. Since the discharge duration increases from 8.0 to 11.97 h, the lower instantaneous net power alone

does not establish a decrease in daily electrical energy output. In contrast, Q_{HW} represents the 24 h equivalent heat output, and its reduction corresponds to lower daily heat production.

Consequently, the obtained solution represents a balanced compromise between thermodynamic performance and economic competitiveness. Overall, the proposed multi-objective optimization effectively improves the efficiency and cost performance of the GT-molten salt TES-CCES integrated system and provides a more favorable operating strategy for multi-period energy management in terms of the two stated optimization objectives.

Table 11. Comparison of the baseline and optimized operating conditions and system performance.

Variable	Baseline	Optimized	Improvement
Pressure ratio of Comp2	15.0	15.01	-
Inlet temperature of Turb2 (K)	1473.15	1629.31	-
Pressure of HPT (MPa)	27.0	30.32	-
Charge/Discharge time (h)	8.0	11.97	-
Isentropic efficiency of the Turb1 (%)	90.0	91.96	-
Isentropic efficiency of the Turb2 (%)	88.0	91.99	-
η_{el} (%)	48.71	53.99	+10.84%
η_{en} (%)	75.97	77.37	+1.84%
η_{ex} (%)	50.29	54.82	+9.01%
$W_{net,inst}$ (MW)	40.26	36.55	−9.21%
Q_{HW} (MW)	14.13	12.19	−13.73%
c_{ptot} ($·GJ^{-1})	14.32	13.55	−5.38%

4.6. Comparison with Existing Integrated Energy Storage Systems

To further demonstrate the characteristics of the proposed system, a comparison with representative integrated energy storage systems reported in recent studies is presented in Table 12. The comparison focuses on the system configuration, storage technology, analysis method, optimization strategy, and research objective.

Table 12. Comparison of the proposed system with representative integrated energy storage systems reported in the literature.

Ref.	System Configuration	Analysis	Operation	Optimization	Contribution
Samson et al. [43]	GTCC + TES	Energy, Exergy, TEA	Daily	-	Flexibility
Cao et al. [44]	CCGT + TES	Thermodynamic	Daily	-	Peak regulation
Zhao et al. [45]	sCO_2 + TES + CCES	Thermo-economic	Single	-	Storage comparison
Dewevre et al. [2]	CCES	Review	-	-	Technology review
This work	GT + TES + CCES	Energy, Exergy, Exergoeconomic	Daily	NSGA-II	Integrated optimization

As shown in Table 12, previous studies mainly focused on improving the operational flexibility of gas turbine systems through molten salt thermal energy storage or evaluating different CCES configurations. Although integrated thermal storage and CCES technologies have been investigated, comprehensive thermo-economic optimization considering the coordinated operation of gas turbines, molten salt TES, and CCES has rarely been reported.

Compared with the existing studies, the proposed system combines GT exhaust heat recovery, molten salt thermal storage, and CCES within a unified 24 h operating framework. Furthermore, an integrated energy, exergy, and exergoeconomic analysis is coupled with MOO to simultaneously improve the exergy utilization level and reduce the unit product cost. These features distinguish the proposed system from previously reported configurations and demonstrate its potential for efficient and flexible integrated energy utilization.

5. Conclusions

In this study, an integrated GT-TES-CCES system with cascade utilization of GT exhaust heat was proposed. A comprehensive thermodynamic and exergoeconomic model was developed to evaluate the system performance considering the different operating periods of the continuously operated GT subsystem and periodically operated CCES subsystem. A unified 24 h evaluation framework was introduced to consistently assess the energy, exergy, and economic characteristics of the integrated system. The main conclusions are as follows:

1. The proposed GT-TES-CCES system effectively integrates power generation, molten salt TES, CCES, and heat recovery through cascade utilization of GT exhaust heat. The developed unified 24 h evaluation framework enables a consistent comparison between continuously operated components and periodically operated charging/discharging processes, providing a suitable methodology for the thermodynamic and exergoeconomic analysis of integrated energy systems with different operating schedules.
2. Under the design condition, the system achieves an η_{el} of 48.71%, an η_{en} of 75.97%, an η_{ex} of 50.29%, an Q_{HW} of 14.13 MW, and an $W_{net,inst}$ of 40.26 MW during the discharge period. These results demonstrate that the integration of TES and CCES enables flexible energy utilization while improving the comprehensive utilization of gas turbine exhaust heat.
3. The exergy analysis indicates that the combustor exhibits the highest exergy destruction among individual components, while the gas turbine subsystem and heat exchangers also contribute considerable irreversibility. The exergoeconomic analysis further reveals the cost formation characteristics of each component, with the combustor contributing the highest exergy destruction cost. These results provide insights into the optimization potential of the integrated system.
4. The sensitivity analysis reveals that the PR, turbine inlet temperature, high-pressure CO_2 storage pressure, charging/discharging time, and the isentropic efficiencies of both turbines significantly influence the system performance. Increasing the PR, turbine inlet temperature, and storage pressure improves the exergy efficiency, whereas extending the charging/discharging duration mainly reduces the product unit exergy cost by improving equipment utilization.
5. A MOO was performed to maximize the η_{ex} while minimizing the c_{ptot}. Compared with the baseline design, the optimized configuration increases the η_{el} from 48.71% to 53.99%, improves the η_{ex} from 50.29% to 54.82%, and reduces the c_{ptot} from 14.32 to 13.55 \$·GJ^{-1}, demonstrating a favorable thermodynamic-economic compromise.

Overall, the proposed GT-TES-CCES system demonstrates considerable potential for improving the flexibility and comprehensive utilization of gas turbine energy systems. Future work will focus on dynamic operation under variable load conditions, experimental validation, and the incorporation of renewable energy sources to further enhance system adaptability and practical applicability.

https://doi.org/10.3390/app162110854

Author Contributions: Conceptualization, L.T., X.L., D.W., Y.X. and D.Z.; methodology, L.T., X.L. and D.W.; software, L.T. and X.L.; validation, D.W., Y.X. and D.Z.; investigation, L.T. and X.L.; resources, Y.X. and D.Z.; writing—original draft preparation, L.T. and X.L.; writing—review and editing, L.T. and D.W.; visualization, L.T. and X.L.; supervision, Y.X. and D.Z. All authors have read and agreed to the published version of the manuscript.

Funding: This research was funded by the Shanghai Municipal Science and Technology Major Project.

Institutional Review Board Statement: Not applicable.

Informed Consent Statement: Not applicable.

Data Availability Statement: The data supporting the findings of this study are not publicly available but are available from the corresponding author upon reasonable request.

Conflicts of Interest: Luyi Tan is employed by the Shanghai XuanYuan Power Technology Co., Ltd. The remaining authors declare that the research was conducted in the absence of any commercial or financial relationships that could be construed as a potential conflict of interest.

Abbreviations

The following abbreviations are used in this manuscript:

Abbreviations		Ch	Chemical
CCES	CO_2 Energy Storage System	k	The index of component
GT	Gas turbine	F	Fuel
TES	Thermal energy storage	ph	physical
c_{ptot}	Total unit product exergy cost	P	Product
sCO_2	Supercritical CO_2	*1,2,…*	State points
SPECO	Specific Exergy Costing	*discharging*	Discharging process
MOO	Multi-objective optimization	*charge*	Charging process
Comp	Compressor	**Nomenclature**	
Turb	Turbine	η	Isentropic efficiency
HE	Heat exchanger	η_{ex}	Exergy efficiency
CST	Cold storage tank	η_{el}	Electrical efficiency
HST	Hot storage tank	η_{en}	Overall energy efficiency
LPT	Low-pressure tank	h	Specific enthalpy
HPT	High-pressure tank	W	Power
Comb	Combustor	m	Mass flow rate
NSGA-II	Non-dominated Sorting Genetic Algorithm II	Q	Heat energy
TIT	Turbine inlet temperature	T	Temperature
PR	Pressure ratio	P	Pressure
GTCC	Gas turbine combined cycle	$\dot{E}$	Exergy
Subscripts		s	Specific entropy
out	Outlet	$\mathcal{E}$	Exergy efficiency
in	Inlet	$\dot{C}$	Exergy flow cost
s	Isentropic process	c	Unit exergy flow cost
cc	Combustor Chamber	CRF	Capital recovery factor
0	Environment state	N	Operating time
h	Hot	n	System lifetime
c	Cold	r	relative cost difference
HW	Hot water	f	Exergoeconomic factor
eq	equivalent	CC	Closeness coefficient
D	Destruction	d	Distance

References

1. Shamsi, S.S.M.; Barberis, S.; Maccarini, S.; Traverso, A. Large Scale Energy Storage Systems Based on Carbon Dioxide Thermal Cycles: A Critical Review. *Renew. Sustain. Energy Rev.* **2024**, *192*, 114245. https://doi.org/10.1016/j.rser.2023.114245.
2. Dewevre, F.; Lacroix, C.; Loubar, K.; Poncet, S. Carbon Dioxide Energy Storage Systems: Current Researches and Perspectives. *Renew. Energy* **2024**, *224*, 120030. https://doi.org/10.1016/j.renene.2024.120030.
3. Xu, W.; Zhao, P.; Gou, F.; Wu, W.; Liu, A.; Wang, J. A Combined Heating and Power System Based on Compressed Carbon Dioxide Energy Storage with Carbon Capture: Exploring the Technical Potential. *Energy Convers. Manag.* **2022**, *260*, 115610. https://doi.org/10.1016/j.enconman.2022.115610.
4. Fan, G.; Lu, X.; Chen, K.; Zhang, Y.; Han, Z.; Yu, H.; Dai, Y. Comparative Analysis on Design and Off-Design Performance of Novel Cascade CO_2 Combined Cycles for Gas Turbine Waste Heat Utilization. *Energy* **2022**, *254*, 124222. https://doi.org/10.1016/j.energy.2022.124222.
5. Jiang, Y.; Ma, Y.; Han, F.; Ji, Y.; Cai, W.; Wang, Z. Assessment and Optimization of a Novel Waste Heat Stepped Utilization System Integrating Partial Heating sCO_2 Cycle and Ejector Refrigeration Cycle Using Zeotropic Mixtures for Gas Turbine. *Energy* **2023**, *265*, 126326. https://doi.org/10.1016/j.energy.2022.126326.
6. Xu, W.; Zhao, P.; Liu, A.; Wu, W.; Wang, J. Design and Off-Design Performance Analysis of a Liquid Carbon Dioxide Energy Storage System Integrated with Low-Grade Heat Source. *Appl. Therm. Eng.* **2023**, *228*, 120570. https://doi.org/10.1016/j.applthermaleng.2023.120570.
7. Tang, J.; Li, Q.; Werle, S.; Wang, S.; Yu, H. Development and Comprehensive Thermo-Economic Analysis of a Novel Compressed CO_2 Energy Storage System Integrated with High-Temperature Thermal Energy Storage. *Energy* **2024**, *303*, 131941. https://doi.org/10.1016/j.energy.2024.131941.
8. Hao, J.; Zheng, P.; Li, Y.; Zhang, Z.; Zhang, J.; Yang, J.; Yue, Y.; Li, X. Study on the Operational Feasibility Domain of Combined Heat and Power Generation System Based on Compressed Carbon Dioxide Energy Storage. *Energy* **2024**, *291*, 130122. https://doi.org/10.1016/j.energy.2023.130122.
9. Jiang, Y.; Li, B.; Su, W.; Wang, S. Aeroderivative Gas Turbine Integrated with Supercritical CO_2 Cycle for Gas-to-Power: Comprehensive Assessment and Optimization. *Energy* **2025**, *334*, 137662. https://doi.org/10.1016/j.energy.2025.137662.
10. Sun, R.; Liu, M.; Zhao, Y.; Yan, J. Proposal Design and Thermodynamic Analysis of a Coal-Fired sCO_2 Power System Integrated with Thermal Energy Storage. *J. Energy Storage* **2024**, *82*, 110495. https://doi.org/10.1016/j.est.2024.110495.
11. Sohrabi, A.; Asgari, N.; Imran, M.; Wakil Shahzad, M. Comparative Energy, Exergy, Economic, and Environmental (4E) Analysis and Optimization of Two High-Temperature Kalina Cycles Integrated with Thermoelectric Generators for Waste Heat Recovery from a Diesel Engine. *Energy Convers. Manag.* **2023**, *291*, 117320. https://doi.org/10.1016/j.enconman.2023.117320.
12. Bagdanavicius, A.; Ali, A.M.; Barbour, E.R.; De Oliveira Junior, M.M.; Pottie, D.L.; Garvey, S.; Baniamerian, Z.; Hough, E. Exergoeconomic Evaluation of Adiabatic Compressed Air Energy Storage: Effects of Pressure Ratio and Configuration. *J. Energy Storage* **2025**, *138*, 118662. https://doi.org/10.1016/j.est.2025.118662.
13. Li, H.; Li, Z.; Lee, S.; Lu, Y.; Ju, Y.; Zhang, C. Supercritical Carbon Dioxide Cycle Thermodynamic and Exergoeconomic Improvements Using a Bidirectional Coupling Strategy. *Energy* **2024**, *296*, 131140. https://doi.org/10.1016/j.energy.2024.131140.
14. He, T.; Cao, Y.; Si, F. Thermodynamic Analysis and Optimization of a Compressed Carbon Dioxide Energy Storage System Coupled with a Combined Heating and Power Unit. *Energy Convers. Manag.* **2023**, *277*, 116618. https://doi.org/10.1016/j.enconman.2022.116618.
15. Liu, Z.; Guan, H.; Jin, X.; Su, W.; Shao, J.; Fan, J.; Zhang, H.; Li, H.; Sun, D. Thermodynamic and Economic Analysis of a Trans-Critical CO_2 Energy Storage System Integrated with ORC and Solar Energy. *Energy* **2024**, *313*, 133667. https://doi.org/10.1016/j.energy.2024.133667.
16. Zhao, R.; Liu, Z. Thermo-Economic Performance of a Compressed CO_2 Energy Storage System with a Flexible Gas Holder. *J. Energy Storage* **2023**, *60*, 106675. https://doi.org/10.1016/j.est.2023.106675.
17. Liu, X.; Wang, D.; Xie, Y.; Zhang, D.; Wang, C.; Zhou, Z.; Zhao, M. Thermodynamic and Exergoeconomic Analysis and Multi-Objective Optimization of a Novel Tank-Free Transcritical CO_2 Energy Storage System. *Energy* **2026**, *344*, 139846. https://doi.org/10.1016/j.energy.2025.139846.
18. Liu, X.; Wang, D.; Xie, Y.; Zhang, D. Performance Assessment of a Compressed CO_2 Energy Storage System with Absorption Refrigeration Cycle. *J. Energy Storage* **2026**, *178*, 123618. https://doi.org/10.1016/j.est.2026.123618.
19. Jeong, J.H.; Park, H.S.; Park, Y.K.; Kim, T.S. Analysis of the Influence of Hydrogen Co-Firing on the Operation and Performance of the Gas Turbine and Combined Cycle. *Case Stud. Therm. Eng.* **2024**, *54*, 104061. https://doi.org/10.1016/j.csite.2024.104061.

20. Kaya, M. Air Excess Coefficient and Irreversibility Value Analysis of Gas Turbines. *Period. Polytech. Mech. Eng.* **2024**, *68*, 312–319. https://doi.org/10.3311/PPme.23779.
21. Amiri Rad, E.; Kazemiani-Najafabadi, P. Thermo-Environmental and Economic Analyses of an Integrated Heat Recovery Steam-Injected Gas Turbine. *Energy* **2017**, *141*, 1940–1954. https://doi.org/10.1016/j.energy.2017.11.044.
22. Sun, L.; Wang, D.; Xie, Y. Energy, Exergy and Exergoeconomic Analysis of Two Supercritical CO_2 Cycles for Waste Heat Recovery of Gas Turbine. *Appl. Therm. Eng.* **2021**, *196*, 117337. https://doi.org/10.1016/j.applthermaleng.2021.117337.
23. Wang, D.; Sun, L.; Xie, Y. Performance Evaluation of CO_2 Pressurization and Storage System Combined with S–CO_2 Power Generation Process and Absorption Refrigeration Cycle. *Energy* **2023**, *273*, 127197. https://doi.org/10.1016/j.energy.2023.127197.
24. Yang, H.; Gallagher, R.; Chartrand, P.; Gheribi, A.E. Development of a Molten Salt Thermal Conductivity Model and Database for Advanced Energy Systems. *Sol. Energy* **2023**, *256*, 158–178. https://doi.org/10.1016/j.solener.2023.04.009.
25. Yin, S.; Zheng, K.; Bai, C.; Yan, X.; Liu, Z. A Constant Pressure Compressed CO_2 Energy Storage with Water Compensating: Comprehensive Thermo-Economic Analysis. *Energy* **2025**, *332*, 137269. https://doi.org/10.1016/j.energy.2025.137269.
26. Fu, Y.; Cai, L.; Liu, C.; Wu, M.; Guan, Y. Thermodynamic and Economic Performance Comparison of Biomass Gasification Oxy-Fuel Combustion Power Plant in Different Gasifying Atmospheres Using Advanced Exergy and Exergoeconomic Approach. *Renew. Energy* **2024**, *226*, 120290. https://doi.org/10.1016/j.renene.2024.120290.
27. Balakheli, M.M.; Mehregan, M.; Hashemian, S.M. Energy, Exergy, Exergoeconomic and Exergoenvironmental Evaluation of a Combined Power, Cooling and Steam Generation System with Biomass Source and Different Gasification Agents. *Energy Convers. Manag.* **2026**, *347*, 120537. https://doi.org/10.1016/j.enconman.2025.120537.
28. Sheng, J.; Voldsund, M.; Ertesvåg, I.S. Advanced Exergy Analysis of the Oil and Gas Processing Plant on an Offshore Platform: A Thermodynamic Cycle Approach. *Energy Rep.* **2023**, *9*, 820–832. https://doi.org/10.1016/j.egyr.2022.12.021.
29. Lazzaretto, A.; Tsatsaronis, G. SPECO: A Systematic and General Methodology for Calculating Efficiencies and Costs in Thermal Systems. *Energy* **2006**, *31*, 1257–1289. https://doi.org/10.1016/j.energy.2005.03.011.
30. Caliskan, H.; Ekici, S.; Sohret, Y. Advanced Exergy Analysis of the Turbojet Engine Main Components Considering Mexogenous, Endogenous, Exegenous, Avoidable and Unavoidable Exergy Destructions. *Propuls. Power Res.* **2022**, *11*, 391–400. https://doi.org/10.1016/j.jppr.2022.07.002.
31. Ghaebi, H.; Parikhani, T.; Rostamzadeh, H. Energy, Exergy and Thermoeconomic Analysis of a Novel Combined Cooling and Power System Using Low-Temperature Heat Source and LNG Cold Energy Recovery. *Energy Convers. Manag.* **2017**, *150*, 678–692. https://doi.org/10.1016/j.enconman.2017.08.052.
32. Sun, R.; Zhao, Y.; Liu, M.; Yan, J. Thermodynamic Design and Optimization of Pumped Thermal Electricity Storage Systems Using Supercritical Carbon Dioxide as the Working Fluid. *Energy Convers. Manag.* **2022**, *271*, 116322. https://doi.org/10.1016/j.enconman.2022.116322.
33. Hançer Güleryüz, E.; Özen, D.N. Advanced Exergy and Exergo-Economic Analyses of an Advanced Adiabatic Compressed Air Energy Storage System. *J. Energy Storage* **2022**, *55*, 105845. https://doi.org/10.1016/j.est.2022.105845.
34. Cui, J.; Yang, X.; Yang, Z.; Liang, W.; Xie, J. Design Optimization and Development of an Explainable Multi-Objective Optimization Framework: A-CAES System Integrated with Advanced Thermal Energy Storage. *Energy Convers. Manag.* **2026**, *352*, 121095. https://doi.org/10.1016/j.enconman.2026.121095.
35. Zhang, W.; Wu, C.; Deng, T. Comprehensive Thermo-Economic Analysis and Discharging-Scheme Optimization of Advanced Adiabatic Compressed Air Energy Storage Systems. *J. Energy Storage* **2026**, *179*, 123745. https://doi.org/10.1016/j.est.2026.123745.
36. Michalski, S.; Hanak, D.P.; Manovic, V. Techno-Economic Feasibility Assessment of Calcium Looping Combustion Using Commercial Technology Appraisal Tools. *J. Clean. Prod.* **2019**, *219*, 540–551. https://doi.org/10.1016/j.jclepro.2019.02.049.
37. Samanta, S.; Ghosh, S. Techno-Economic Assessment of a Repowering Scheme for a Coal Fired Power Plant through Upstream Integration of SOFC and Downstream Integration of MCFC. *Int. J. Greenh. Gas Control* **2017**, *64*, 234–245. https://doi.org/10.1016/j.ijggc.2017.07.020.
38. Wang, S.; Liu, C.; Li, J.; Sun, Z.; Chen, X.; Wang, X. Exergoeconomic Analysis of a Novel Trigeneration System Containing Supercritical CO_2 Brayton Cycle, Organic Rankine Cycle and Absorption Refrigeration Cycle for Gas Turbine Waste Heat Recovery. *Energy Convers. Manag.* **2020**, *221*, 113064. https://doi.org/10.1016/j.enconman.2020.113064.
39. Zhang, Y.; Shen, X.; Tian, Z.; Yang, C.; Gao, W.; Yang, K. 5E (Energy, Exergy, Energy Level, Exergoeconomic, and Exergetic Sustainability) Analysis on a Carbon Dioxide Binary Mixture Based Compressed Gas Energy Storage System: A Comprehensive Research and Feasibility Validation. *Energy Convers. Manag.* **2023**, *292*, 117399. https://doi.org/10.1016/j.enconman.2023.117399.

40. Sun, L.; Tang, B.; Xie, Y. Performance Assessment of Two Compressed and Liquid Carbon Dioxide Energy Storage Systems: Thermodynamic, Exergoeconomic Analysis and Multi-Objective Optimization. *Energy* **2022**, *256*, 124648. https://doi.org/10.1016/j.energy.2022.124648.
41. Tang, B.; Sun, L.; Xie, Y. Comprehensive Performance Evaluation and Optimization of a Liquid Carbon Dioxide Energy Storage System with Heat Source. *Appl. Therm. Eng.* **2022**, *215*, 118957. https://doi.org/10.1016/j.applthermaleng.2022.118957.
42. Lu, M.; Du, Y.; Yang, C.; Zhang, Z.; Wang, H.; Sun, S. Performance Analysis and Multi-Objective Optimization of a Combined System of Brayton Cycle and Compression Energy Storage Based on Supercritical Carbon Dioxide. *Appl. Therm. Eng.* **2024**, *236*, 121837. https://doi.org/10.1016/j.applthermaleng.2023.121837.
43. Samson, M.B.; Lunda, A.I.W. Enhancing Flexibility in a 550 MW Gas Turbine Combined Cycle Power Plant Through Molten-Salt Thermal Energy Storage. *Energy Storage* **2026**, *8*, e70432. https://doi.org/10.1002/est2.70432.
44. Cao, L.; Yu, J.; Wang, L.; Xu, X. Combined Cycle Gas Turbine System with Molten Salt Energy Storage: Peak Regulation and Flexibility. *Processes* **2025**, *13*, 604. https://doi.org/10.3390/pr13030604.
45. Zhao, Y.; Chang, Z.; Zhao, Y.; Yang, Q.; Liu, G.; Li, L. Performance Comparison of Three Supercritical CO_2 Solar Thermal Power Systems with Compressed Fluid and Molten Salt Energy Storage. *Energy* **2023**, *282*, 128807. https://doi.org/10.1016/j.energy.2023.128807.

Disclaimer/Publisher's Note: The statements, opinions and data contained in all publications are solely those of the individual author(s) and contributor(s) and not of MDPI and/or the editor(s). MDPI and/or the editor(s) disclaim responsibility for any injury to people or property resulting from any ideas, methods, instructions or products referred to in the content.